Journal of Medicinal Chemistry

Article

pubs.acs.org/jmc

Hydrophilic, Potent, and Selective 7-Substituted 2-Aminoquinolines as Improved Human Neuronal Nitric Oxide Synthase Inhibitors

Anthony V. Pensa,[†,⊥] Maris A. Cinelli,[†,⊥] Huiying Li,[‡] Georges Chreifi,[‡] Paramita Mukherjee,[†] Linda J. Roman,[§] Pavel Martásek,[§,∥] Thomas L. Poulos,*[,‡] and Richard B. Silverman*[,†]

[†]Department of Chemistry, Department of Molecular Biosciences, Chemistry of Life Processes Institute, Center for Molecular Innovation and Drug Discovery, Northwestern University, Evanston, Illinois 60208-3113, United States

[‡]Departments of Molecular Biology and Biochemistry, Pharmaceutical Sciences, and Chemistry, University of California, Irvine, California 92697-3900, United States

[§]Department of Biochemistry, University of Texas Health Science Center, San Antonio, Texas 78384-7760, United States

[∥]Department of Pediatrics and Center for Applied Genomics, First School of Medicine, Charles University and BIOCEV 121 08 Prague, Czech Republic

Supporting Information

ABSTRACT: Neuronal nitric oxide synthase (nNOS) is a target for development of antineurodegenerative agents. Most nNOS inhibitors mimic L-arginine and have poor bioavailability. 2-Aminoquinolines showed promise as bioavailable nNOS inhibitors but suffered from low human nNOS inhibition, low selectivity versus human eNOS, and significant binding to other CNS targets. We aimed to improve human nNOS potency and selectivity and reduce off-target binding by (a) truncating the original scaffold or (b) introducing a hydrophilic group to interrupt the lipophilic, promiscuous pharmacophore and promote interaction with human nNOS-specific His342. We synthesized both truncated and polar 2-aminoquinoline derivatives and assayed them against recombinant NOS enzymes. Although aniline and pyridine derivatives interact with His342, benzonitriles conferred the best rat and human nNOS inhibition. Both introduction of a hydrophobic substituent next to the cyano group and aminoquinoline methylation considerably improved isoform selectivity. Most importantly, these modifications preserved Caco-2 permeability and reduced off-target CNS binding.

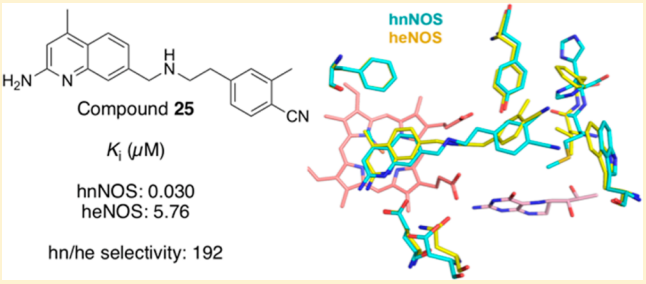

INTRODUCTION

Neurodegenerative disorders (such as Alzheimer's and Parkinson's diseases, among others) result in severe neurological, cognitive, and motor deficits. The prevalence of these diseases has increased over the past century, and this upward trend is predicted to continue, especially with an increasingly aged population,[1] making the development of therapeutic agents to treat these disorders a priority. In addition, the neuronal damage observed in these diseases can also be observed in patients with neuropathic pain, stroke, cerebral palsy, and head trauma.

We have been investigating the enzyme neuronal nitric oxide synthase (nNOS) as a potential target for antineurodegenerative therapeutics. In the brain, nitric oxide (NO, produced by nNOS) is needed for neuronal signaling, but under conditions of neurodegeneration, NO levels are high, owing to overexpressed or unregulated nNOS. This increased NO can form reactive species such as peroxynitrite, leading to neuronal cell damage.[2] Indeed, nNOS[3−6] has been implicated in the pathogenesis of neurodegeneration and peripheral nerve dysfunction (neuropathic pain), and inhibition of nNOS has shown promise in treating or preventing neuronal damage in animal models.[7,8]

NO is formed when homodimeric nNOS converts L-arginine to L-citrulline, which occurs in the enzyme's oxygenase domain. Electrons (from NADPH) are shuttled through redox cofactors (FAD and FMN) in the reductase domain and then move from one monomer's reductase domain to the other's oxygenase domain,[9] where electron transfer proceeds to (6*R*)-5,6,7,8-tetrahydrobiopterin (H_4B) and finally to heme, which then oxidizes the bound L-arginine.[10] Along with nNOS, two other isoforms of NOS (inducible NOS, or iNOS, and endothelial NOS, or eNOS) make NO in humans. iNOS is involved in the immune response, whereas the NO produced by eNOS regulates smooth muscle tone and blood pressure.

Over the years, several classes of nNOS inhibitors have been developed in our laboratories (**1**−**6** are representative examples, Figure 1).[11−15] These compounds are all competitive with L-arginine; compound **3** is also a heme-iron coordinator.[12]

Received: June 7, 2017

DOI: 10.1021/acs.jmedchem.7b00835
J. Med. Chem. XXXX, XXX, XXX−XXX

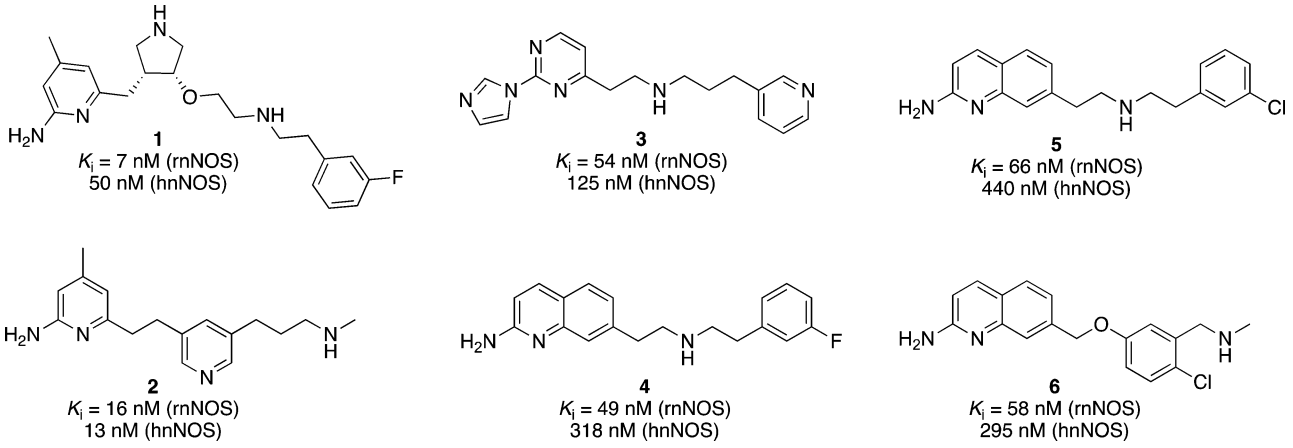

Figure 1. Previously designed human nNOS inhibitors.

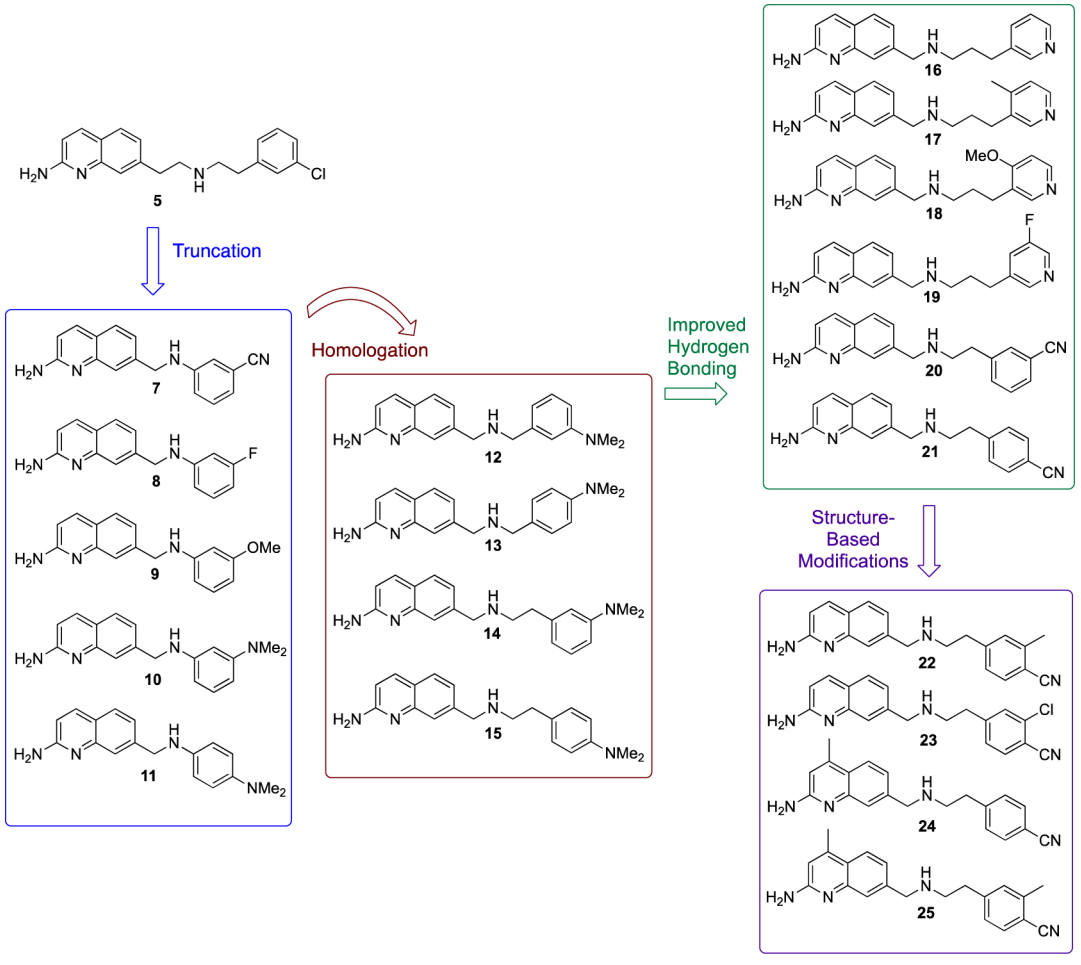

Figure 2. Overall strategy for design of hydrophilic 2-aminoquinolines based on lead **5**.

A general challenge in development of arginine-mimetic inhibitors is that molecules that resemble arginine often possess chemical properties (basicity, H-bonding potential, and high polar surface area, or PSA) that impede oral bioavailability and passage through the blood–brain barrier (BBB; compounds **1**, **2**, and **6**, for example, have poor Caco-2 permeability).

In addition to having good BBB permeability, nNOS inhibitors must be selective for the neuronal isoform over iNOS and eNOS. For example, eNOS inhibition can cause cardiovascular problems and hypertension.[16] Nonspecific iNOS inhibition could interfere with immune defense, but its role in the brain is more complex; one study indicated that mice lacking iNOS develop enhanced Alzheimers' pathology,[17] while others indicate that iNOS inhibition could actually be neuroprotective.[18] A more recent challenge has been designing inhibitors with high potency against human nNOS (hnNOS). Historically, many structure-based design efforts have utilized rat nNOS (rnNOS), so many compounds (such as most shown in Figure 1) are selective for the rat enzyme, leading to weaker

DOI: 10.1021/acs.jmedchem.7b00835
J. Med. Chem. XXXX, XXX, XXX−XXX

hnNOS inhibitors with low selectivity over human eNOS (heNOS).

The 2-aminoquinolines (compounds **4**–**6**) have shown considerable promise as a scaffold for further nNOS inhibitor development. Compounds **4** and **5** have good potency, selectivity, and cellular permeability.[14] They also exhibit good oral bioavailability in mice (**4**) and brain penetration in rats (**5**). Unfortunately, compound **5**, considered our best lead for further development, had an unfavorable safety profile in rats, where it caused neurological and cardiovascular side effects at the doses required for effective nNOS inhibition. Counter-screening against a variety of CNS targets via the Psychoactive Drug Screening Program's (PDSP's) radioligand binding assay[19] revealed that **5**, with its GPCR-ligand-like pharmacophore, is a promiscuous binder (affinity <100 nM) at serotonin, opioid, and histamine receptors, and its scaffold also resembles known human ether-a-go-go-related-gene (hERG) channel blockers. It is imperative that specific CNS-acting NOS inhibitors not strongly bind numerous other targets in the brain, as this could cause neurological, psychological, or other side effects. Additionally, compound **5** (and **4**) has poor hnNOS activity and low hnNOS/heNOS (hn/he) selectivity.

One strategy for reducing the off-target binding of these compounds involved rearranging the pharmacophore of **5** to disrupt the GPCR ligand-like core, leading to compounds such as **6**,[15] where the position of the polar amine and hydrophobic aryl group are "inverted" relative to **5**. Unfortunately, this compound had much lower cellular permeability and its hnNOS activity, while improved from **5**, was still low, as was its hn/he selectivity. We therefore, in addition to our newer studies on phenyl-ether linked aminoquinolines,[15,20] sought alternative (and parallel) strategies for reducing the off-target binding of **5** and improving its hnNOS activity and hn/he selectivity.

One such strategy, detailed therein, is based on a key structural difference between rnNOS and hnNOS. While rnNOS possesses an isoform-specific hydrophobic pocket, consisting of Tyr706, Leu337, and Met336, hnNOS lacks the leucine residue, which is replaced by His342.[21] This pocket in hnNOS is smaller and more polar,[22] and preliminary crystallography studies indicated that the hydrophobic haloaryl tail of **4**, responsible for much of this compound's stabilization when bound to the hydrophobic pocket of rnNOS,[14] is not well-accommodated in the analogous region of hnNOS (possibly because of the bulky and polar histidine), resulting in the loss of hydrophobic contacts and much lower hnNOS activity. Our initial strategy consisted of simply truncating the linker chain between the quinoline and the hydrophobic aryl ring, hoping that lack of repulsion between the aryl ring and His342 might improve the selectivity for hnNOS over rnNOS (as observed for truncated 2-aminopyridines).[23]

To this end, compounds **7**–**11** (Figure 2), bearing substituents on the aryl ring capable of a wide variety of interactions, were prepared and assayed against rnNOS and hnNOS. Although less active against these isoforms compared to compounds **4**–**6** (Table 1, vide infra), the good rat/human (rn/hn) selectivity of dimethylamines **10** and **11** encouraged the development of a second strategy, to *directly* interact with His342 itself.

The pyridine of compound **3** was reported to H-bond with His342 (discovered via X-ray crystallographic analysis),[13] improving this scaffold's hnNOS potency. To this end, we prepared several series of compounds with hydrophilic groups that could act as H-bond acceptors: homologated *N*,*N*-dimethylamino derivatives (**12**–**15**), pyridine derivatives (**16**–**19**), and nitriles **20**–**21**. Finally, structure-based modifications were performed to improve the hn/he selectivity of nitrile **21**. The *o*-methyl group (of **22**) and *o*-chlorine (of **23**) were installed on the benzonitrile ring to make additional contact with Met336 (in rnNOS; Met341 in hnNOS). This residue is absent in eNOS isoforms (both bovine and human eNOS), replaced by a smaller valine, and contact between methionine residues (vs valine residues) and inhibitors has previously been implicated in improved n/e selectivity.[14,15,22] Finally, two active nitrile-containing molecules (**22** and **23**) were methylated at the 4-position of the quinoline. This modification was previously reported to improve potency (and sometimes n/e selectivity) for the analogous 2-aminopyridines by the interaction of the 4-methyl group with a small hydrophobic pocket located near the "back wall" of the heme-binding pocket.[24]

In addition to possibly improving hnNOS activity, it was hypothesized that the addition of more hydrophilic groups (such as amines, pyridines, or nitriles) could reduce off-target binding. For example, the addition of a nitrile (relative to an aromatic chloride, as in **5**) slightly increases the PSA and decreases the overall hydrophobicity of the molecule,[25] which may (a) disfavor binding to GPCRs and other CNS targets, many of which depend on extensive hydrophobic interactions for ligand binding, and (b) decrease nonspecific hydrophobic interactions with other proteins. As very high PSA (>100 Å^2) could hamper brain permeation or oral bioavailability, however, we were careful to keep the PSA of all analogues below 80 Å^2.

All synthesized compounds were assayed against rnNOS and hnNOS to determine their selectivity for the human isoform (Table 1). To determine selectivity, murine iNOS and bovine eNOS were used, and select compounds were also assayed against human eNOS in an attempt to begin translating our work to more "humanized" systems (Table 2). Finally, the most selective compound (**25**) was assayed in a Caco-2 assay to approximate cellular permeability and in the PDSP counter-screen to determine the effects of the new modifications on off-target binding.

CHEMISTRY

Preparation of 7-substituted 2-aminoquinolines **7**–**13** proceeded through bromide **26**, which was prepared according to literature procedures.[14,15] To prepare truncated analogues **7**–**11** (Scheme 1) bromide **26** was treated with an excess of commercially available anilines **27**–**31** and catalytic potassium iodide under microwave conditions[26] to afford the acetamide-protected intermediates **32**–**36** in good yields. These intermediates were not characterized extensively but were immediately deacetylated with K_2CO_3 in refluxing methanol,[27] followed by treatment with methanolic HCl to yield desired analogues **7**–**11** as hydrochloride salts. The homologated compounds (**12** and **13**) were prepared by treatment of **26** with commercially available benzylamines **37** or **38** in the presence of Cs_2CO_3 (Scheme 2).[28] The desired products were Boc-protected at the secondary amine to aid in purification, providing protected intermediates **39** (from **37**) and **40** (from **38**). Subsequent deacetylation, workup, and cleavage of the Boc group under acidic conditions afforded **12** and **13**, respectively.

To synthesize aminoquinolines possessing more than one methylene unit between the aryl ring and the secondary amine (analogues **14**–**16**, **20**, and **21**), the requisite primary amines

DOI: 10.1021/acs.jmedchem.7b00835
J. Med. Chem. XXXX, XXX, XXX−XXX

Scheme 1[a]

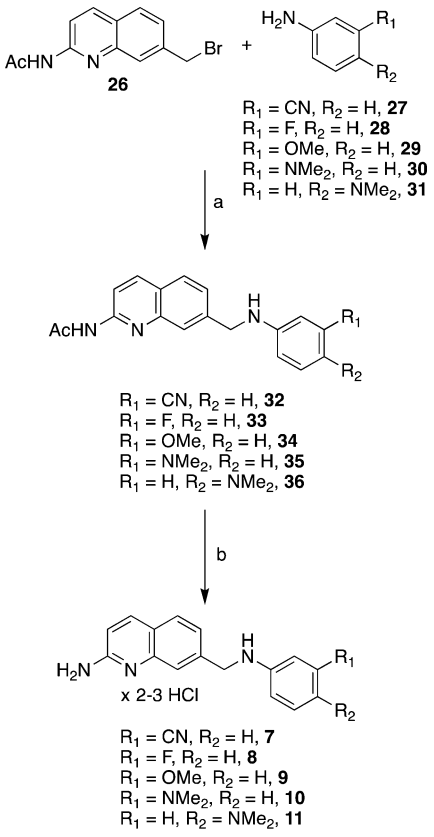

[a]Reagents and conditions: (a) cat. KI, MeCN, 110 °C, μ-wave; (b) (*i*) K_2CO_3, MeOH, reflux, (*ii*) MeOH/HCl, rt (after isolation).

Scheme 2[a]

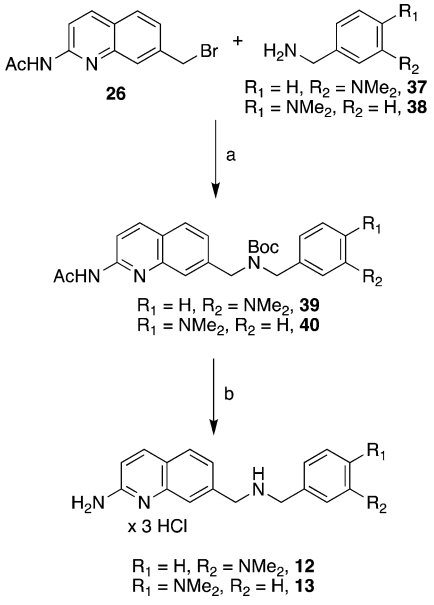

[a]Reagents and conditions: (a) (*i*) Cs_2CO_3, DMF, rt, (*ii*) Boc_2O, THF, rt; (b) (*i*) K_2CO_3, MeOH, reflux, (*ii*) MeOH/HCl, rt (after isolation).

44, **47**, **50**, and **53** were first prepared. To prepare phenethylamine **44**, nitroarene **41** (Scheme 3A) was first hydrogenated to yield aniline **42**,[29] followed by Eschweiler–Clarke methylation and hydrogenation of **43** to afford **44**. To prepare isomeric amine **47** (Scheme 3B), commercially available aldehyde **45** was condensed with nitromethane to yield unstable nitrostyrene **46**,[30] which was immediately reduced to **47** with $LiAlH_4$.[31] Pyridinepropanamine **50** (Scheme 3C) was prepared by the method of Mukherjee et al.,[13] starting with the Mitsunobu conversion of primary alcohol **48** to azide **49**, followed by Staudinger reduction to the amine (and acidic hydrolysis to yield dihydrochloride salt **50**).

Finally, cyanophenethylamine **53** (Scheme 3D) was prepared by Boc-protection of commercially available 3-bromophenethylamine (**51**) followed by palladium-catalyzed cyanation of intermediate carbamate **52**. Removal of the Boc group yielded hydrochloride **53**.[32]

From these amines, as well as commercially available 4-cyanophenethylamine (**55**), analogues **14**–**16**, **20**, and **21** were prepared by an indirect reductive amination (Scheme 4) where aldehyde **54** (prepared by literature procedures)[15] was treated with the required primary amine under mildly acidic, dehydrating conditions (cat. AcOH and anhydrous Na_2SO_4), and the resulting imine was reduced with $NaBH_4$ (and the secondary amine protected with Boc_2O to aid in purification as described above) to yield intermediates **56**–**60**. These were deprotected to yield final compounds **14**–**16**, **20**, and **21**.

To prepare substituted pyridine compounds **17**–**19**, the necessary pyridinepropanamines were prepared from bromopyridines **61**–**63** (Scheme 5). Sonogashira coupling with *N*-Boc-propargylamine yielded alkynes **64**–**66**, which were hydrogenated and deprotected to give dihydrochloride salts **67**–**69**. Subsequent indirect reductive amination between these amines and **54**, followed by reduction and protection, gave the intermediate acetamides **70**–**72**. Deacetylation and Boc group removal afforded pyridine derivatives **17**–**19** as water-soluble trihydrochloride salts.

The substituted cyanophenethylamines (**81** and **82**) and their respective aminoquinoline derivatives **22** and **23** were prepared as shown in Scheme 6. Starting with commercially available methyl 4-bromo-3-methylbenzoate (**73**, for **81**) and 4-bromo-3-chlorobenzoic acid (**74**, for **82**), reduction with either $LiAlH_4$ or BH_3–THF, respectively, resulted in primary alcohols **75** and **76**.[33,34] Subsequent bromination of the alcohol under Appel conditions and displacement of the bromide with KCN resulted in benzonitrile intermediates **77**[35] and **78** in good yield. BH_3–THF reduction[36] and protection with Boc_2O afforded **79** and **80**.

Palladium-catalyzed cyanation of **79** followed by deprotection (vide supra) yielded the hydrochloride salt **81**. Likely because of the bulk of the *o*-chloro substituent, the analogous cyanation was very low-yielding, and **82** was instead prepared by reaction with CuCN in refluxing DMF followed by acidic deprotection (to yield the crude hydrochloride salt). Subsequent indirect reductive amination with **54** and either **81** or **82**, followed by $NaBH_4$ reduction and Boc-protection, yielded protected intermediates **83** and **84**.

Deprotection, as described above, afforded **22** and **23** in moderate yield. Synthesis of 4-methylated aminoquinolines[37] **24** and **25** (Scheme 7) began with Doebner–Miller condensation of 3-bromoaniline **85** and 3-buten-2-one to yield **86**, and oxidation with *m*-CPBA resulted in *N*-oxide **87**. Deoxygenative amination (and debutylation of the intermediate *t*-butylaminoquinoline with TFA)[38] yielded **88**. Acetylation with *N*-acetylimidazole yielded **89**, followed by Pd-catalyzed formylation[39] to yield **90**. A similar indirect reductive amination between **90** and either **55** or **81**, followed by reduction and

DOI: 10.1021/acs.jmedchem.7b00835
J. Med. Chem. XXXX, XXX, XXX–XXX

Scheme 3[a]

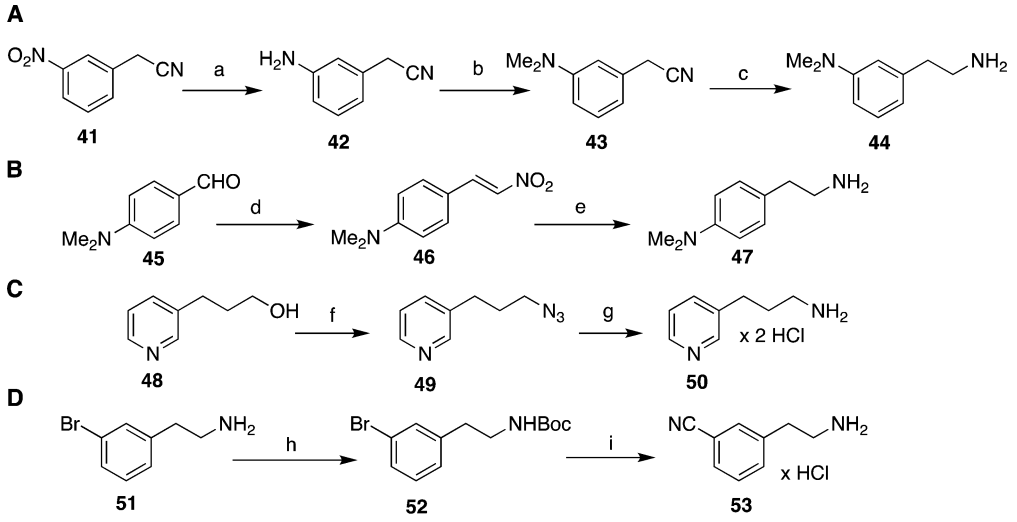

[a]Reagents and conditions: (a) H_2, Pd/C, MeOH, rt; (b) formalin, HCO_2H, DMF, 0 °C–reflux; (c) H_2, Raney Ni, MeOH/NH_3:EtOH (1:1), rt; (d) NO_2CH_3, NH_4OAc, AcOH, reflux; (e) $LiAlH_4$ in THF. 0 °C–reflux; (f) PPh_3, diphenylphosphoryl azide, DIAD, THF, 0 °C–rt; (g) (*i*) $P(OEt)_3$, benzene, reflux, (*ii*) MeOH/HCl, rt (after isolation); (h) Boc_2O, THF, rt; (i) (*i*) $K_4[Fe(CN)_6]$, *t*-BuXPhos Pd G_3, *t*-BuXPhos, dioxane, KOAc (0.1 M in H_2O), reflux, (*ii*) MeOH/HCl, rt (after isolation).

Scheme 4[a]

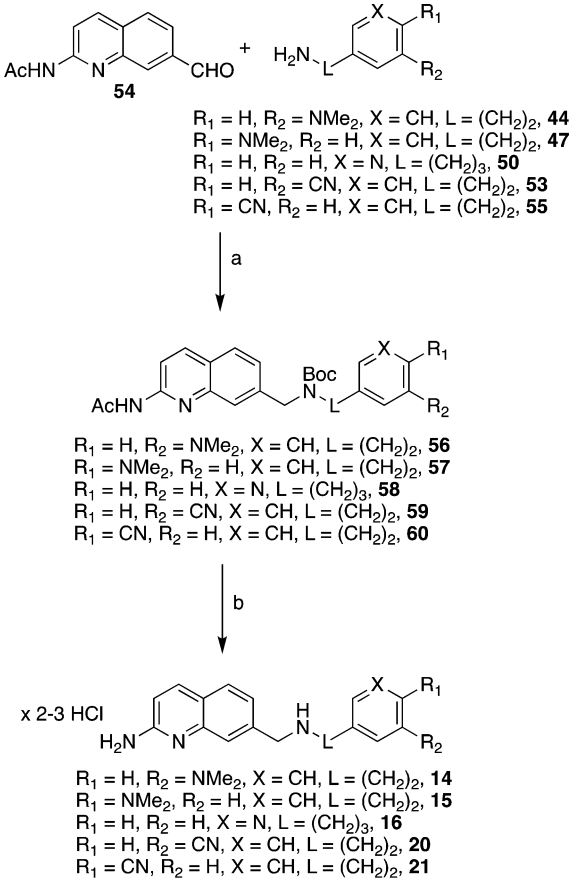

[a]Reagents and conditions: (a) (*i*) Et_3N first, or AcOH, Na_2SO_4, $CHCl_3$, rt, (*ii*) $NaBH_4$, MeOH, 0 °C–rt, (*iii*) Boc_2O, THF, rt; (b) (*i*) K_2CO_3, MeOH, reflux, (*ii*) MeOH/HCl, rt (after isolation).

protection, afforded protected intermediates **91** and **92**, which were then deprotected to yield **24** and **25** as the dihydrochloride salts.

Scheme 5[a]

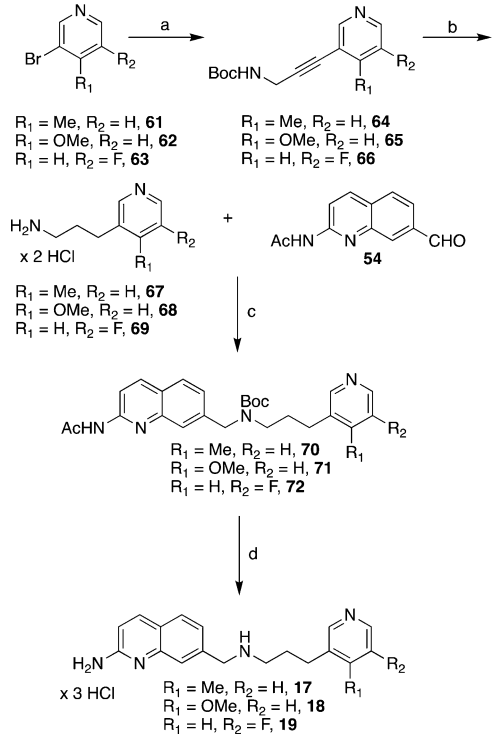

[a]Reagents and conditions: (a) *N*-Boc-propargylamine, CuI, PPh_3, $Pd(PPh_3)_2Cl_2$, Et_3N, 90 °C; (b) (*i*) H_2, Pd/C, MeOH, rt, (*ii*) MeOH/HCl, rt (after isolation); (c) (*i*) AcOH, Na_2SO_4, $CHCl_3$, rt, (*ii*) $NaBH_4$, MeOH, 0 °C–rt, (*iii*) Boc_2O, THF, rt; (d) (*i*) K_2CO_3, MeOH, reflux, (*ii*) MeOH/HCl, rt (after isolation).

RESULTS AND DISCUSSION

Historically, rat nNOS (rnNOS) and bovine eNOS (beNOS) were the first NOS enzymes to be expressed and crystallized and to date have provided a majority of the structural data for

DOI: 10.1021/acs.jmedchem.7b00835
J. Med. Chem. XXXX, XXX, XXX–XXX

Scheme 6[a]

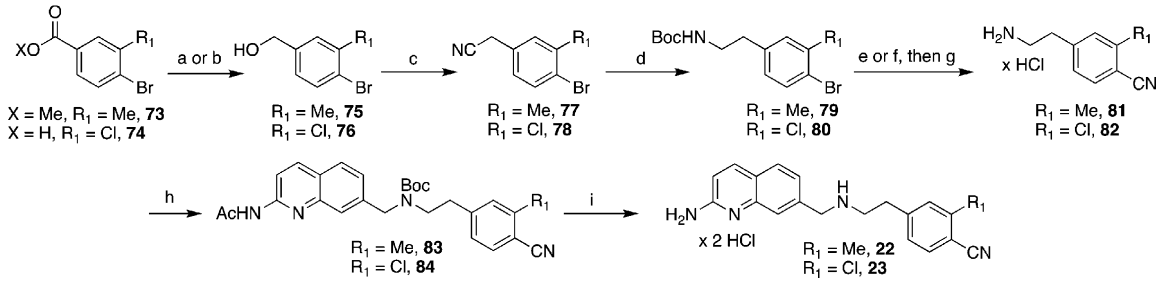

[a]Reagents and conditions: (a) (for **73**) $LiAlH_4$ in THF, THF, −15 °C; (b) (for **74**) BH_3−THF, THF, 0 °C−rt; (c) (*i*) CBr_4, PPh_3, DCM, 0 °C, (*ii*) KCN, Bu_4NBr, CH_2Cl_2, H_2O, rt; (d) (*i*) BH_3−THF, THF, reflux, (*ii*) Boc_2O, THF, rt; (e) (for **78**) $K_4[Fe(CN)_6]$, *t*-BuXPhos Pd G3, *t*-BuXPhos, dioxane, KOAc (0.1 M in H_2O), 100 °C; (f) (for **79**) CuCN, DMF, reflux; (g) MeOH/HCl, rt (after isolation); (h) (*i*) **54**, AcOH, Na_2SO_4, $CHCl_3$, rt, (*ii*) $NaBH_4$, MeOH, 0 °C−rt, (*iii*) Boc_2O, THF, rt; (i) (*i*) K_2CO_3, MeOH, reflux, (*ii*) MeOH/HCl, rt (after isolation).

Scheme 7[a]

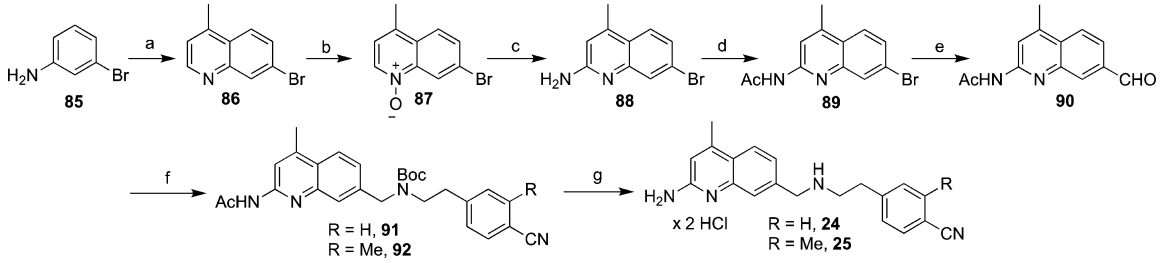

[a]Reagents and conditions: (a) 3-buten-2-one, $FeCl_3·6H_2O$, AcOH, 60 °C−140 °C; (b) *m*-CPBA, CH_2Cl_2, rt; (c) (*i*) *t*-$BuNH_2$, Ts_2O, $PhCF_3$/CH_2Cl_2, 0 °C, (*ii*) TFA, reflux; (d) *N*-acetylimidazole, THF, reflux; (e) *N*-formylsaccharin, Et_3SiH, $Pd(OAc)_2$, dppb, Na_2CO_3, DMF, 75 °C; (f) (*i*) **55** or **81**, AcOH, Na_2SO_4, $CHCl_3$, rt, (*ii*) $NaBH_4$, MeOH, 0 °C, rt, (*iii*) Boc_2O, THF, rt; (g) (*i*) K_2CO_3, MeOH, reflux, (*ii*) MeOH/HCl, rt (after isolation).

isoform-selective inhibitor design. Therefore, compounds **7**−**25** were first assayed against rnNOS, murine macrophage iNOS (miNOS), and beNOS, using the previously described hemoglobin capture assay (see Experimental Section). These isoforms are also used to approximate isoform selectivity for rnNOS because the amino acids that generally interact with our inhibitors are identical in rat and murine iNOS, as well as in rat and bovine eNOS, and are unlikely to result in significant species differences. Because of our 2-fold goal of decreasing the off-target binding and improving the human nNOS (hnNOS) activity of the previous leads, the studied compounds were also assayed against purified hnNOS, and six of the most potent compounds against hnNOS were also assayed against purified human eNOS (heNOS). Table 1 summarizes the apparent K_i values and isoform selectivities for **7**−**25**, and the activity and selectivity for hnNOS and heNOS are summarized in Table 2. Values for **4**−**6** are included for comparison. We have found human iNOS very difficult to express and purify in our laboratories, so it is not included in this discussion. As such, most of the following discussion will focus on nNOS and eNOS, as achieving high n/e selectivity was a primary goal of this study. Additionally, iNOS isoforms do not easily grow diffraction-quality crystals, the role of iNOS in neurodegeneration is complicated, and n/e selectivity tends to be much harder to achieve than n/i selectivity for 2-aminoquinolines.

Our initial attempts at improving the hnNOS activity of the 2-aminoquinoline scaffold involved truncation of the aminoalkyl linker to remove the clash between His342 in hnNOS and the bulky haloaryl groups of **4** and **5**. The truncated derivatives (**7**−**10**), however, were significantly less potent than **4** and **5** against rnNOS, with the most potent derivative (**7**) showing approximately 10-fold less activity than **4** and **5** (Table 1).

Initial Structural Analysis of Truncated and Aniline Analogues. The X-ray crystal structure of compound **8** (which was used for crystallographic analysis because of the poor solubility of **7**) reveals the reason for the K_i increase for these truncated inhibitors (Figure 3A). While the aminoquinoline portion mimics arginine and binds to Glu592 (rnNOS), there are no interactions with the nNOS-specific hydrophobic pocket (Leu337, Met336, and Tyr706) that provided a major source of stabilization upon binding of **4** and **5**. Instead, the fluorophenyl ring points upward toward the roof of the active site near Arg481, where the fluorine interacts with Gln478. This "bent-up" binding mode was previously observed for aniline-linked aminoquinoline derivatives,[15] reflecting the geometry required for the aniline to interact with the nearby heme propionate. The larger methoxyl group of **9** and the *N*,*N*-dimethylamine of **10** should be similarly positioned, but owing to the larger size of these substituents (relative to the fluorine in **8**), the potency for **9** and **10** is lower.

Not too surprisingly, **8** has similar potency against rnNOS and hnNOS, given that the binding mode is the same (see the hnNOS-**8** structure in Figure 3B). The rnNOS/hnNOS selectivity approaches 1:1, and in addition to an identical binding mode to rnNOS, there are no direct interactions with His342 in the hnNOS-**8** structure. Despite their low potency, similar rnNOS/hnNOS activity is also observed for **10** and **11**, and this, along with the increased hydrophilicity, prompted further investigation of the *N*,*N*-dimethylaniline-containing scaffold.

DOI: 10.1021/acs.jmedchem.7b00835
J. Med. Chem. XXXX, XXX, XXX−XXX

Table 1. Inhibition of NOS Enzymes by Aminoquinoline Analogues 7−25[a]

	K_i (μM)[a]				selectivity	
compd	rnNOS	hnNOS	miNOS	beNOS	rn/mi	rn/be
4	0.049	0.318	44.0	11.2	899	228
5	0.066	0.440	28.4	7.24	431	110
6	0.058	0.295	27.7	12.5	478	216
7	0.529	2.05	15.3	7.95	29	15
8	0.575	0.768	NT	NT	ND	ND
9	1.32	2.17	NT	NT	ND	ND
10	4.83	4.30	NT	NT	ND	ND
11	1.82	1.10	NT	NT	ND	ND
12	0.421	1.02	30.1	6.53	71	16
13	0.522	0.764	42.2	8.42	81	16
14	0.085	0.076	13.3	NT	156	ND
15	0.036	0.274	10.0	1.57	278	44
16	0.038	0.108	11.2	1.04	295	27
17	0.090	0.130	13.8	0.562	153	7
18	0.050	0.073	17.2	1.86	344	37
19	0.216	0.164	84.2	NT	390	ND
20	0.041	0.050	25.0	0.273	609	7
21	0.037	0.032	21.3	0.581	575	16
22	0.021	0.020	10.3	0.092	492	4
23	0.031	0.021	5.15	0.115	166	4
24	0.019	0.052	4.70	1.22	247	64
25	0.025	0.030	4.83	0.468	193	19

[a]Compounds **7**−**25** were assayed in vitro against four purified NOS isoforms: rat nNOS, human nNOS, bovine eNOS, and murine iNOS, using known literature methods, and K_i values were calculated directly from IC_{50} values using the Cheng−Prusoff equation (see Experimental Section for details). IC_{50} values are the average of at least two replicates from 7 to 9 data points; all experimental standard error values are less than 16%, and all correlation coefficients are >0.83. Selectivity values are ratios of respective K_i values. NT = not tested; ND = not determined.

Table 2. Inhibition of hnNOS and heNOS by Selected Compounds[a]

	K_i (μM)[a]		
compd	human nNOS	human eNOS	selectivity (hn/he)
4	0.318	9.49	30
5	0.440	11.8	27
6	0.295	7.41	25
18	0.073	1.58	22
21	0.032	1.03	32
22	0.020	2.08	104
23	0.021	2.70	129
24	0.052	5.79	111
25	0.030	5.76	192

[a]Compounds **18** and **21**−**25** were assayed in vitro against human eNOS, using known literature methods and K_i values were calculated directly from IC_{50} values using the Cheng−Prusoff equation (see Experimental Section for details). IC_{50} values are the average of at least two replicates from 7 to 9 data points; all experimental standard error values are less than 15%, and all correlation coefficients are >0.94. Selectivity values are ratios of respective K_i values; human nNOS K_i values are from Table 2.

Further modification of **10** and **11** (via homologation) resulted in *meta*-substituted compound **12** and *para*-substituted **13**. Both compounds displayed improved potency against rnNOS and hnNOS, with similar K_i values between the two nNOS enzymes, although a greater increase in potency was observed for homologation of **10** to **12**. The rnNOS-**13** and hnNOS-**13** structures (Figure 4A and B, respectively; the rnNOS-**12** and hnNOS-**12** structures are shown in Supporting Information, Figures S1A and B, respectively) indicate that homologation of **11** to **13** does result in additional interactions between the inhibitor and the enzyme.

For example, although the electron density is weak in this area, one *N*-methyl group of **13** can potentially interact with Leu337 and Met336 in rnNOS (Figure 4A). In hnNOS, the *N*,*N*-dimethylamino group prefers an orientation facing away from the polar and bulkier His342 (Figure 4B), instead making contacts with Met341. The linker amine H-bonds with the heme propionates in hnNOS but bends away from the propionates in rnNOS. This difference is likely the result of the different nature of the interactions between the tail *N*,*N*-dimethylamino group and either the polar His342 (hnNOS) or nonpolar Leu337 (rnNOS). Nonetheless, there are some deleterious interactions that may be present as well. The steric crowding around the linker amino group and repulsion of the heme propionates by the nearby phenyl ring make this ring and its substituent partially disordered, as evidenced by the rather poor density in the region (Figure 4B).

Unfortunately, this singly homologated scaffold does not appear to offer significant advantages, potency- or selectivity-wise, over a compound such as **8** (Table 1). Compared to the truncated (**7**−**11**) or singly homologated (**12** and **13**) analogues, the doubly homologated compounds **14** and **15** are significantly improved rnNOS and hnNOS inhibitors. In the rnNOS-**15** structure (Figure 5A), the good potency of **15** is visible in the clean electron density throughout the inhibitor except for the *N*,*N*-dimethylamino group. The main reasons for increased potency are that the elongated tail relieves the clash and crowding around the linker amino group, allowing the H-bond with heme propionate D, and there are nonpolar interactions between the aryl ring and *N*,*N*-dimethylamino group and Met336 and Trp306. The hnNOS-**15** structure is very much the same, except the aryl ring moves over slightly so that it is farther away from Met341 (>4.2 Å) while the *N*,*N*-dimethylamino group interacts with His342. Compound **15** thus provides another example where the His342/Leu337 difference between hnNOS and rnNOS, respectively, controls differences in affinity. Compound **15** makes better nonpolar contacts with Leu337 and Met336 in rnNOS than His342 and Met341 in hnNOS, which explains why it is still a better rnNOS inhibitor.

Compound **15** has the best rn/be selectivity of the *N*,*N*-dimethylaniline compounds tested. Like the nNOS structures, the beNOS-**15** structure is well ordered (Figure 5C) and retains the H-bonds from the linker amine to both heme propionates. The 44-fold rn/be selectivity is mainly the result of the smaller Val106 in beNOS that replaces Met336 of rnNOS. A glycerol molecule is bound next to Val106 (common in many eNOS structures). The aryl ring moves slightly to avoid the glycerol, and as such, any contacts less than 5.2 Å between the *N*,*N*-dimethylamine and the small Val106 cannot be made, although some hydrophobic contacts with Trp76, Leu107, and Val106 are retained with the aryl ring itself. In contrast, the close hydrophobic contacts from both the aryl ring and *N*,*N*-dimethylamino group to the nearby Trp306 and bulkier Met336 are more extensive and at shorter distances in rnNOS. Therefore, the rn/be selectivity is likely a true isoform difference (due to Met/Val variation) despite the binding being

DOI: 10.1021/acs.jmedchem.7b00835
J. Med. Chem. XXXX, XXX, XXX−XXX

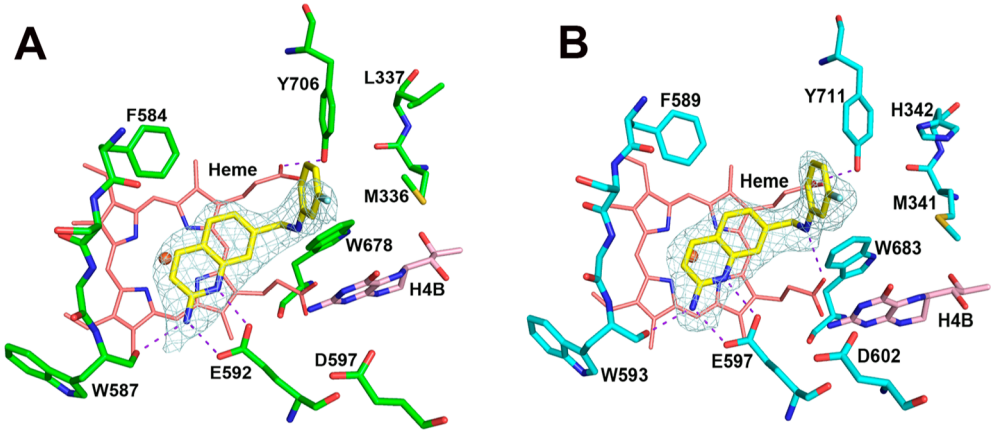

Figure 3. Active site structures of rnNOS-**8** (A) and hnNOS-**8** (B). For clarity, the residues on the roof of the rnNOS active site, Glu478 and Arg481, are not shown. In this figure and all the following structural figures, major H-bonds are depicted with dashed lines. The omit $F_o - F_c$ electron density maps for the bound inhibitor are displayed at 2.5σ contour level. All structural figures were prepared with PyMol (www.pymol.org).

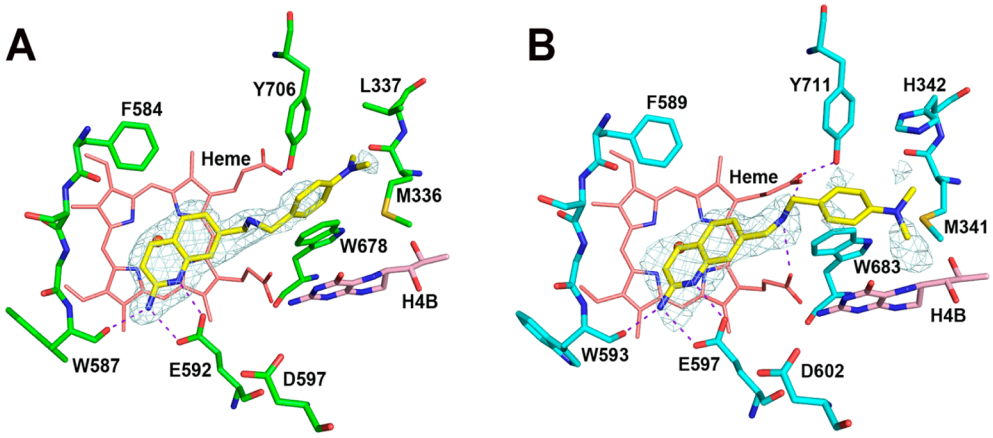

Figure 4. Active site structures of rnNOS-**13** (A) and hnNOS-**13** (B). Note that only in hnNOS can the linker amine of **13** make H-bonds with the heme propionates; however, the *N*,*N*-dimethylaniline is more disordered in hnNOS than in rnNOS (indicated by density quality).

slightly disturbed by glycerol. Compound **15** also has the highest rn/mi selectivity out of the aniline series. Although structural data are not available for miNOS-**15**, miNOS has an asparagine (Asn115) in place of Leu337 in rnNOS, and this residue was previously shown to be a crucial determinant of rn/mi selectivity,[40] as it strongly repels hydrophobic moieties such as aryl rings (or possibly **15**'s aniline methyl groups).

Despite the increased hnNOS activity of these compounds, it is worth noting that there are several drawbacks associated with *N*,*N*-dimethylanilines such as **14** and **15**. Often flagged as metabolic liabilities in drug discovery (because of potential oxidation into toxic species),[41] anilines can also be air or light sensitive. Although we handled all anilines carefully, storing stocks and solutions in the dark and cold and assaying all compound dilutions within 48 h of preparation, it was found that solutions of **14** lost their nNOS inhibitory activity when stored for longer periods of time (ca. 1 week), and a *N*,*N*-diethyl analogue of **11** (not reported here) darkened rapidly in solution. Both of these findings indicated possible instability of the aniline and highlighted the need for other histidine-interacting groups.

Pyridine Analogues. As alternative hydrophilic groups, pyridine analogues **16**–**19** were designed to mimic **3**, which was shown by X-ray crystallography to H-bond with His342 and resulted in good hnNOS inhibiton for pyrimidinylimidazole inhibitors.[13] Compound **16** is not only an excellent rnNOS inhibitor (36 nM), but its hnNOS inhibitory activity is improved 4-fold relative to **5**. In both the rnNOS-**16** (Figure 6A) and hnNOS-**16** structures (Figure 6B), the linker amino group H-bonds with heme propionate D, leaving the tail pyridino group near a mainly hydrophobic pocket. In both structures, the tail pyridino group shows flexibility, indicated by weaker electron density. However, the position of the pyridine ring can be identified at lower contour levels, and the crystal structures indicate that the pyridine can have two functions. In the rnNOS-**16** structure, the pyridine acts as a hydrophobic group, with its aryl hydrogens making van der Waals contacts with Met336, Leu337, and Trp306 (Figure 6A), while in the hnNOS-**16** structure, the pyridine nitrogen forms a 2.8 Å H-bond with His342, as well as hydrophobic contacts with Met341 and Trp311 (Figure 6B). The same binding mode is maintained in beNOS (Figure 6C). As with other inhibitors, the rn/be selectivity (27-fold) may stem from Val106 versus Met336 in rnNOS, as contacts with Val106 in beNOS are less extensive and farther away than those with Met336 in rnNOS.

The substituted pyridines (**17** and **18**) were designed to strengthen the H-bond acceptor potential of the pyridine, whereas **19** was meant to mimic the haloaryl group of **4** and **5**. However, neither the rnNOS nor hnNOS activities correlate with the electronics of the pyridine, suggesting other factors are

DOI: 10.1021/acs.jmedchem.7b00835
J. Med. Chem. XXXX, XXX, XXX−XXX

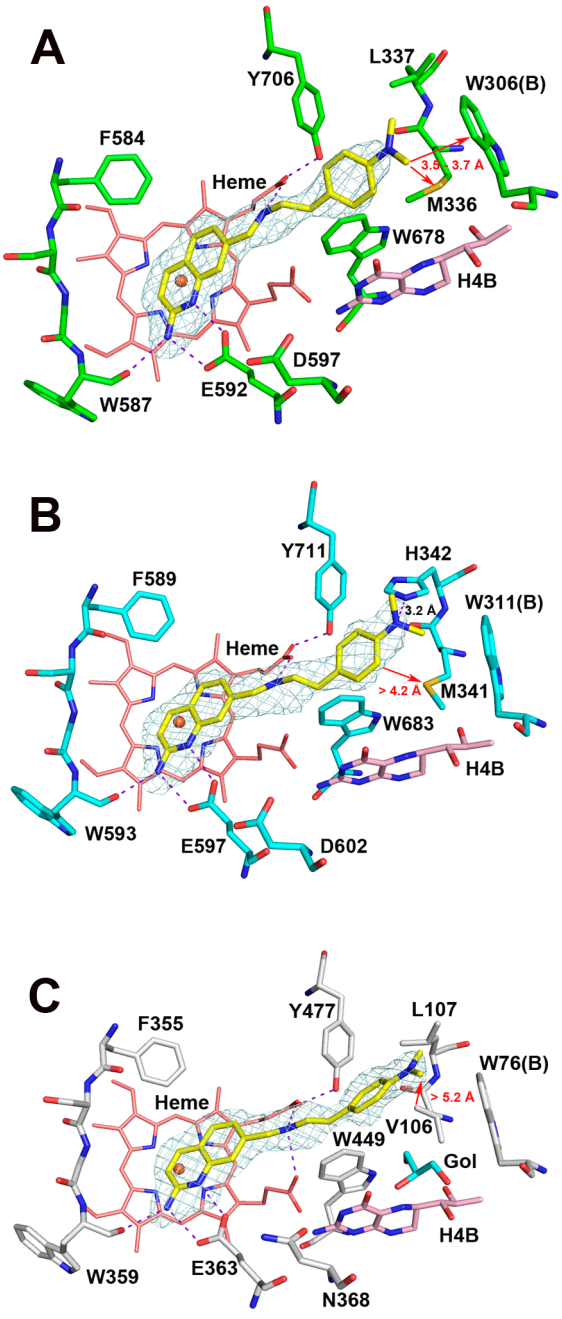

Figure 5. Active site structures of rnNOS-**15** (A), hnNOS-**15** (B), and beNOS-**15** (C). Important van der Waals contacts are marked with red arrows, and distances are labeled in Å. The Trp residue from the other subunit is labeled with a B in parentheses. The glycerol in beNOS is labeled as Gol.

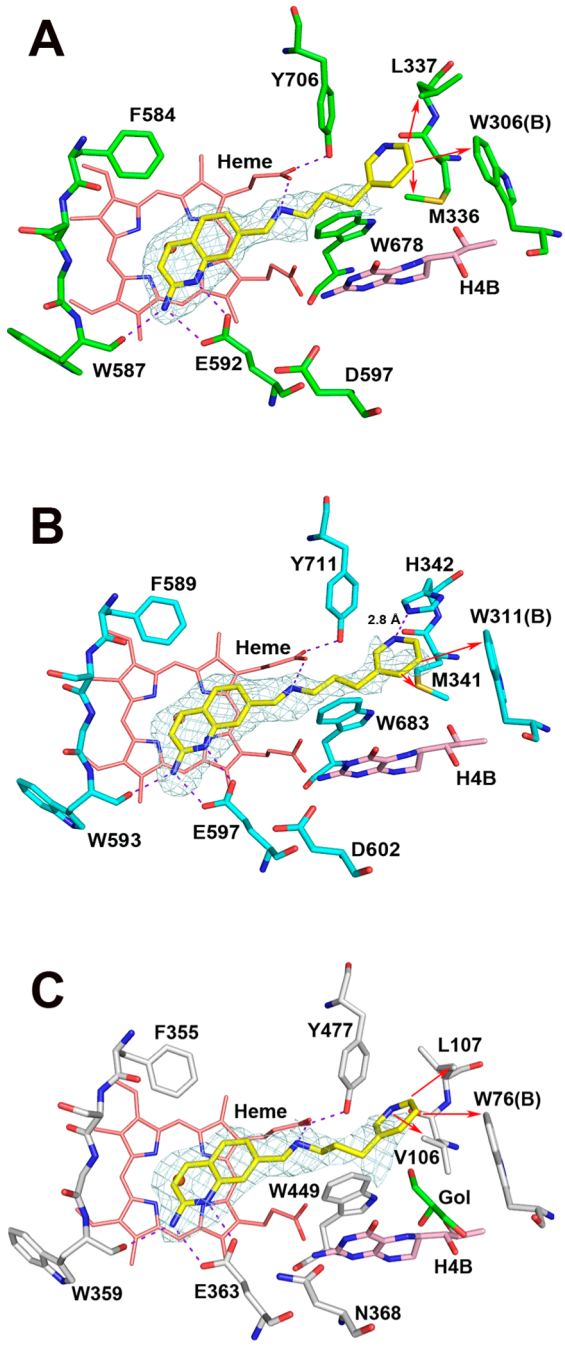

Figure 6. Active site structures of rnNOS-**16** (A), hnNOS-**16** (B), and beNOS-**16** (C). Major van der Waals contacts are marked with red arrows. Gol is a glycerol molecule bound next to H_4B in beNOS.

at play, as revealed by crystallography. In the rnNOS-**17** structure (Supporting Information, Figure S2A), the extra methyl group in **17** contacts Met336, Leu337, and Trp306. In the hnNOS-**17** structure (Supporting Information, Figure S2B), the pyridino group cannot adopt the same orientation, owing to potential close contacts with His342 and thus moves closer to the H_4B site. Similarly, the pyridine ring is oriented differently in the hnNOS-**18** and rnNOS-**18** structures (Figure 7). In the hnNOS-**18** structure, the methoxyl group orients away from His342 and interacts with Met341, whose side chain is repositioned to maximize interactions with the methoxypyridino group (Figure 7A). As **18** is a good hnNOS inhibitor, this is obviously a favorable binding mode. In the rnNOS-**18** structure, the methoxyl group is oriented in the opposite direction, where it forms favorable contacts with Leu337 (Figure 7B).

Inhibitor **19** contains a fluorine, and in the hnNOS-**19** structure (Supporting Information, Figure S3B), this fluorine points toward Met341, while in rnNOS the fluorine faces the opposite direction, toward Leu337. This further underscores that interactions with Met341 are favored in hnNOS, while interactions with Leu337 are favored in rnNOS. As in **16**, a H-bond exists (3.0 Å between the pyridine and His342), although it may be a weaker interaction than in the hnNOS-**16** structure because of the fluorine. Unfortunately, the n/e selectivity for

DOI: 10.1021/acs.jmedchem.7b00835
J. Med. Chem. XXXX, XXX, XXX−XXX

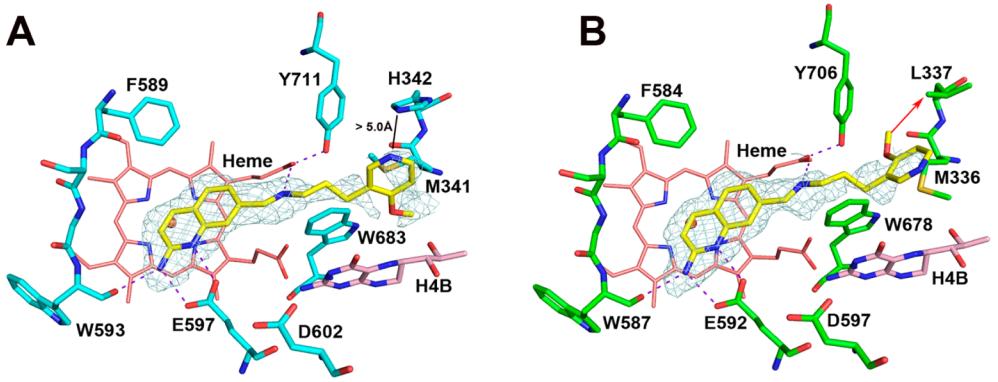

Figure 7. Active site structures of hnNOS-**18** (A) and rnNOS-**18** (B). The distance from the tail pyridino group to His342 is more than 5.0 Å. The methoxyl group makes hydrophobic contact (red arrow) with Leu337 in rnNOS.

these compounds remains quite low. Additionally, compound **18** has very similar K_i values between beNOS and heNOS, indicating that pyridines may bind similarly to the eNOS enzymes of these two species. The pyridine series, however, has good n/i selectivity, suggesting that the pyridino group may also behave as a hydrophobic group in iNOS, clashing with Asn115. Compound **19** is an extremely weak iNOS inhibitor that closely resembles **4**, an analogue that is a similarly poor binder to iNOS.

Benzonitrile Analogues. We also investigated the use of a nitrile as a potential hydrogen-bond acceptor from His342. Compounds **20** and **21** are both potent dual rnNOS and hnNOS inhibitors. However, the hnNOS-**21** (Figure 8A) and rnNOS-**21** structures (Figure 8B) are nearly identical. While the electron density for the cyano group is weak, precluding precise positioning, it is clear that the cyano group does not prefer an orientation that enables strong H-bonding with His342. Instead, in both the rnNOS and rhNOS, the benzonitrile group points toward and contacts Trp311 (hnNOS) or Trp306 (rnNOS). We do, however, observe electron density consistent with a minor conformer where the benzonitrile faces toward His342 (hnNOS) or Leu337 (rnNOS). Computer modeling of the other conformation confirmed that, because of the length of the linker and the bulkiness of the benzonitrile in **21**, even when the cyano group points toward His342 in hnNOS, a H-bond between the two cannot be easily established.

Unfortunately, the rnNOS/beNOS selectivity for **20** and **21** is, like the pyridines, still fairly low. This is mainly because of the tight binding of **21** to beNOS (Table 1). To our surprise, in beNOS the benzonitrile ring actually makes more extensive close contacts with Trp76 and Leu107, as well as the smaller Val106 (Figure 8C). These benzonitrile compounds may simply bind to beNOS too strongly to allow for high rn/be selectivity.

Given the high potency of **20** and **21**, we decided to try several structure-based modifications to improve the n/e selectivity. The *o*-methyl group of **22** and *o*-chlorine of **23** were introduced to provide possible contacts with Met336/Met341 (rnNOS/hnNOS). Interestingly, while this modification does result in a slight improvement in rnNOS and hnNOS potency, it does *not* improve selectivity for rnNOS over beNOS relative to the unsubstituted benzonitrile compounds (**20** and **21**), but it does substantially improve selectivity for hnNOS over heNOS. Both **22** and **23** exhibit hn/he selectivity >100-fold because they bind >20-fold weaker to heNOS than beNOS (Table 1). Examination of the crystal structures revealed a potential reason for this disparity.

In the rnNOS-**22** structure (Figure 9A), the *o*-methyl group turns inward toward Leu337, the phenyl ring and cyano group are approximately 4.2−4.5 Å from Met336, and the cyano group maintains close contacts with Trp306. In the beNOS-**22** structure (Figure 9B), the aryl ring flips over by 180°, where the aryl group contacts (~4.0 Å) Val106 while the cyano group makes similar contacts as in the rnNOS-**22** structure. The similarity in these nonbonded contacts might explain why **22** is the strongest beNOS inhibitor (92 nM) in the series, with a rn/be selectivity of only 4 (Table 1). Similar to observations in other structures, in the hnNOS-**22** structure (Figure 9C), the benzonitrile has turned inward to form a weak H-bond with His342, which places both the aryl ring and extra *o*-methyl group 3.9−4.2 Å from Met341. In the heNOS-**22** structure (Figure 9D), not only is the His342−benzonitrile interaction missing (as His342 is replaced by Phe105), but there is also no interaction between Val104 and the *o*-methyl group of the inhibitor, although the aryl ring does make some contact with Val104. The only obvious difference between heNOS and beNOS that could explain why **22** is a much poorer inhibitor of heNOS than of beNOS is the Phe105 (heNOS) vs Leu107 (beNOS) difference. A similar phenomenon could occur with compound **23** and account for its different potency against beNOS and heNOS (Table 2, Supporting Information, Figure S4). These results suggest that differences in a single residue among the same isoform from different species, such as Leu337/His342 in rnNOS vs hnNOS (and Leu107/Phe105 in beNOS vs heNOS), or even, more importantly, between different isoforms, as Met336/Val104 in hnNOS vs heNOS, can have significant effects on binding of the same compound.

The Effect of Methylation. Finally, a methyl group was introduced at the 4-position of the aminoquinoline to yield compounds **24** and **25** (methylated versions of **21** and **22**, respectively). Previously, this modification was reported to improve potency for 2-aminopyridines[24] by providing an extra hydrophobic contact along the back wall of the heme-binding pocket (an area known as the "S-pocket"). Interestingly, possibly because of the larger size and increased interacting surface area of 2-aminoquinoline in comparison of 2-aminopyridine, the 4-methyl has little effect on potency of these 2-aminoquinoline compounds for nNOS despite the extra hydrophobic contact visible in the crystal structures, such as in the hnNOS-**25** crystal structure (Figure 10A; for the rnNOS-**25** structure see Supporting Information, Figure S5A).

DOI: 10.1021/acs.jmedchem.7b00835
J. Med. Chem. XXXX, XXX, XXX−XXX

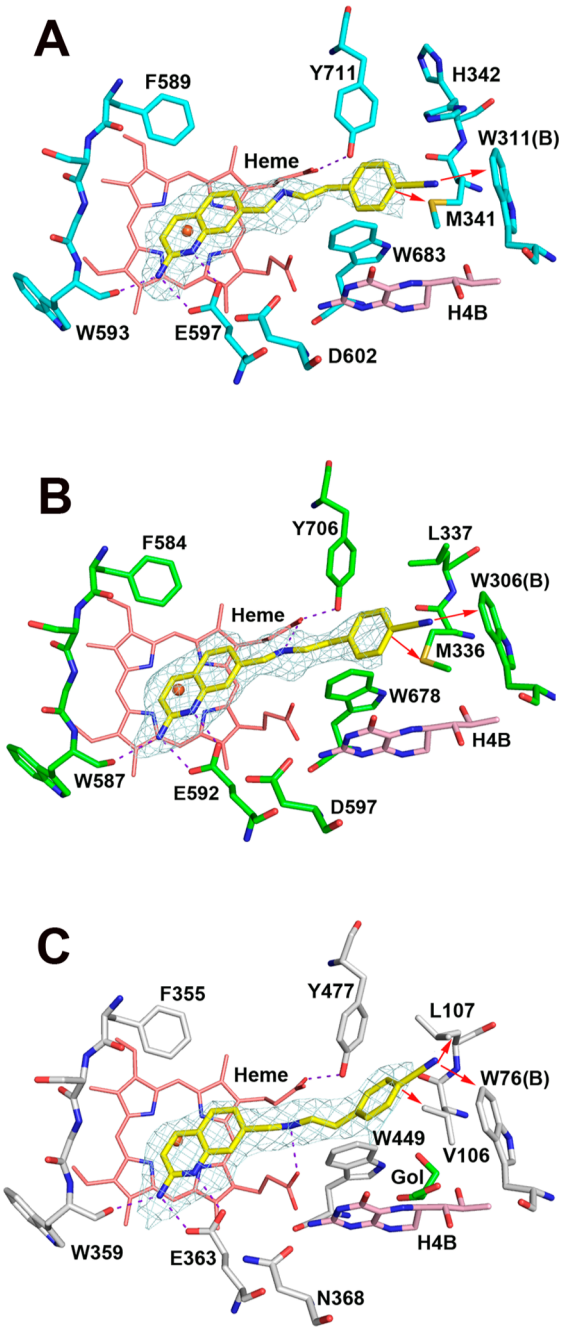

Figure 8. Active site structures of hnNOS-**21** (A), rnNOS-**21** (B), and beNOS-**21** (C). Close van der Waals contacts are marked with red arrows.

How can the 4-methyl group *not* improve potency with this extra contact? In the crystal structures of most of these compounds, a stabilizing H-bond is present between the linker amino group and nearby heme propionate.[13] With the 4-methyl group present, as in the hnNOS-**25** structure, the aminoquinoline's orientation is more parallel with the heme than that in an unmethylated analogue such as **22** (Figure 10C), which possibly strains the linker chain and weakens the H-bond between the amine and propionate. At least for these 2-aminoquinoline compounds, any favorable extra contact with the 4-methyl group may be offset by the weakened H-bond between the linker amine and propionate.

It is worth noting that the 4-methyl group increases n/e selectivity for rnNOS and beNOS, and to a more significant degree, hnNOS and heNOS (the hn/he selectivity for **21** and **22** more than tripled and nearly doubled upon methylation in **24** and **25**, respectively). This increase in selectivity was also reported for 2-aminopyridines[24] although it is not obvious why. For this 2-aminoquinoline scaffold, the improved selectivity is mainly the result of poorer eNOS binding upon adding the 4-methyl group (**22** vs **25**, Table 1). Comparing the heNOS-**25** with the heNOS-**22** structure (Figure 10C) indicates that in addition to the weakened H-bonds with the propionates and the extra contact made by the 4-methyl group (vide supra), there is a difference in the orientation of the *o*-methyl group on the benzonitrile ring, which points toward Phe105 for **25** but away from this residue for **22**. When the 4-methyl group is present, the position of the entire inhibitor (as in **25**) is more sequestered inside the NOS active site due to the extra contact with the protein, and this could introduce steric hindrance and torsional strain in the linker chain or hinder flexibility required to achieve maximal contact. The global effects of all these structural differences lead to poorer binding of the methylated compounds to eNOS, resulting in higher n/e selectivity in general. The trend of increasing selectivity is observed from **21** to **24** as well. The rnNOS-**24**, beNOS-**24**, and heNOS-**24** structures, and the superimposition of **24** and **21** in beNOS, are shown in Supporting Information, Figure S6.

Off-Target Profiling and Cellular Permeability Assay. To assess the efficacy of our modifications in reducing off-target binding, the compound with the highest hn/he selectivity (**25**) was tested in the PDSP (Table 3). In this assay,[19] compounds were tested for binding to 45 different CNS targets and receptors via radioligand displacement. Initially, compounds were tested at a primary high dose (10 μM) and then a secondary K_i determination was performed for compounds showing >50% binding in the primary assay. We have classified off-target binding using the following rubric: *concerning* (K_i < 100 nM, or < ~2× nNOS K_i value), *moderate* (100−300 nM, or ~2−5× nNOS K_i value), *weak* (>300 nM, or > ~5× nNOS K_i value, typically ~1 μM), and *insignificant* (<50% at 10 μM). The off-target profile for **5** reveals concerning or moderate binding at 15/45 targets (mostly serotonin and histamine receptors). There were 22/45 targets that were classified as weak and 8/45 as insignificant for this compound. Conversely, for rearranged compound **6**,[15] the fraction flagged as concerning or moderate decreased, with a concomitant increase in "insignificant" binding. The PDSP results for **25** indicate that the installation of the polar nitrile group is also effective at reducing off-target binding (despite two extra hydrophobic methyl groups on the molecule). Although it is not as effective as **6**'s structural rearrangement, **25** shows only three concerning targets (the 5-HT1a receptor, alpha1A adrenergic receptor, and dopamine D3 receptor) and less overall binding to serotonin receptors, indicating that the polar group may be successfully interrupting the GPCR-ligand-like pharmacophore of **5** or decreasing nonspecific hydrophobic binding. Indeed, it is reported that the installation of polar nitriles reduce overall ligand lipophilicity[42] and, by proxy, may reduce promiscuity and negative toxicological observations relative to isosteric aryl chlorides.[25]

Finally, compound **25** was tested for permeability in a Caco-2 assay (Table 4) to estimate its membrane permeability (such as through the intestinal lumen or the blood−brain barrier, although the efficacy of using Caco-2 to approximate passage

DOI: 10.1021/acs.jmedchem.7b00835
J. Med. Chem. XXXX, XXX, XXX−XXX

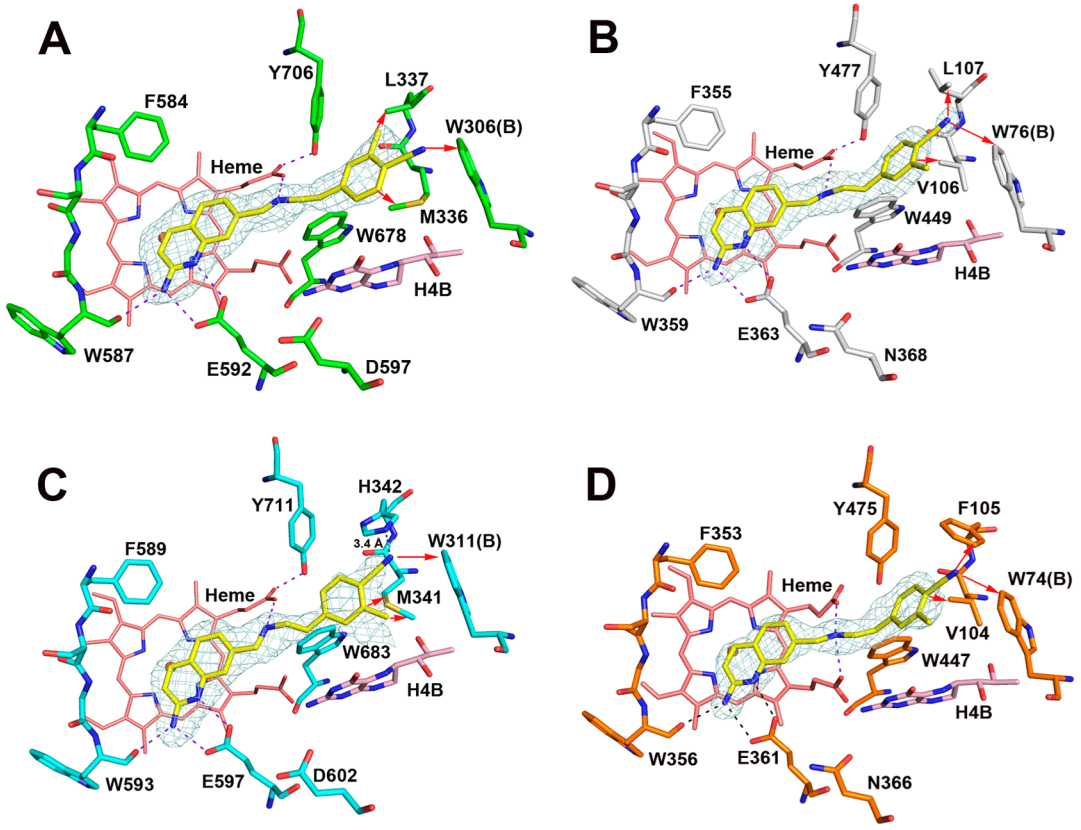

Figure 9. Active site structures of rnNOS-**22** (A), beNOS-**22** (B), hnNOS-**22** (C), and heNOS-**22** (D). van der Waals contacts discussed in the text are marked with red arrows. The weak H-bond mentioned in the text for hnNOS has a distance of 3.4 Å in one subunit but is farther in the other.

through the latter is usually less accurate[43] due to fundamental differences in the two membranes).

Compound **5** is extremely permeable in this assay, has high compound recovery values and a low efflux ratio [ratio of membrane permeability (A → B) to efflux (B → A), <3 is considered favorable]. Pleasingly, despite the hydrophilic modification and increase in total polar surface area (from 50.4 Å^2 for **5** to 74.2 Å^2 for **25**), compound **25** maintains very good permeability, good recovery, and low efflux (indicating that it is unlikely to be a significant substrate for P-gp or other drug efflux transporters).

CONCLUSIONS

In summary, we sought to optimize our first generation of potent and selective 2-aminoquinolines (**4** and **5**) to both (a) improve their binding to hnNOS and selectivity over heNOS, and (b) reduce off-target binding in CNS counter-screening assays by disrupting the GPCR-ligand-like pharmacophore with a hydrophilic group. Although truncation of the scaffold to remove repulsion between the haloaryl moiety and the hnNOS-specific residue His342 did not result in improved potency or selectivity against rnNOS or hnNOS, *N*,*N*-dimethylaniline containing inhibitors had very similar activities against rat and human nNOS. Singly homologating the truncated inhibitors improved this activity slightly, and double homologation significantly improved human nNOS potency. Crystal structures indicated that the *N*,*N*-dimethylaniline could form a weak H-bond with His342. Further improvements in potency were achieved by introduction of a 3-pyridine-containing tail, which could act as both a hydrophobic group (in rnNOS) and H-bond acceptor for His342 (hnNOS), although alternative binding modes were also observed in the crystal structures. The most potent dual rat/human nNOS inhibition (with selectivity of approximately 1:1 between the nNOS enzymes of these two species) was achieved by installation of a nitrile, and selectivity for hnNOS over heNOS was improved to >100-fold by placement of a hydrophobic substituent *ortho*- to the nitrile to interact with Met341 (which is replaced by a smaller valine in heNOS). Interestingly, this modification did not improve selectivity for rnNOS over beNOS. Finally, we found that introduction of a methyl group at position 4 of the aminoquinoline of our most potent benzonitrile-containing leads, while not able to improve potency much toward nNOS, was able to enhance n/e selectivity (both rnNOS/beNOS and hnNOS/heNOS). One compound, the doubly methylated benzonitrile **25**, had nearly 200-fold hnNOS/heNOS selectivity, although, based on the crystal structures, interpretation of this observation is not that straightforward. Compound **25**, when assayed in the PDSP screen, displayed a marked reduction in off-target binding (relative to **5**) without compromising the excellent Caco-2 permeability of the first-generation compounds, indicating that cyanated tail moieties of this type may be useful for designing new bioavailable dual rnNOS/hnNOS inhibitors with improved safety profiles.

EXPERIMENTAL SECTION

General Procedures. Anhydrous solvents (MeOH, DMF, CH_2Cl_2, and THF) were distilled prior to use. All remaining solvents and reagents were purchased from commercial vendors and were used without further purification. Methanolic HCl (3 M, for Boc-deprotection and ammonium salt formation) was prepared fresh by the reaction of acetyl chloride and anhydrous MeOH at 0 °C. Air- or moisture-sensitive reactions were run under an atmosphere of dry

DOI: 10.1021/acs.jmedchem.7b00835
J. Med. Chem. XXXX, XXX, XXX−XXX

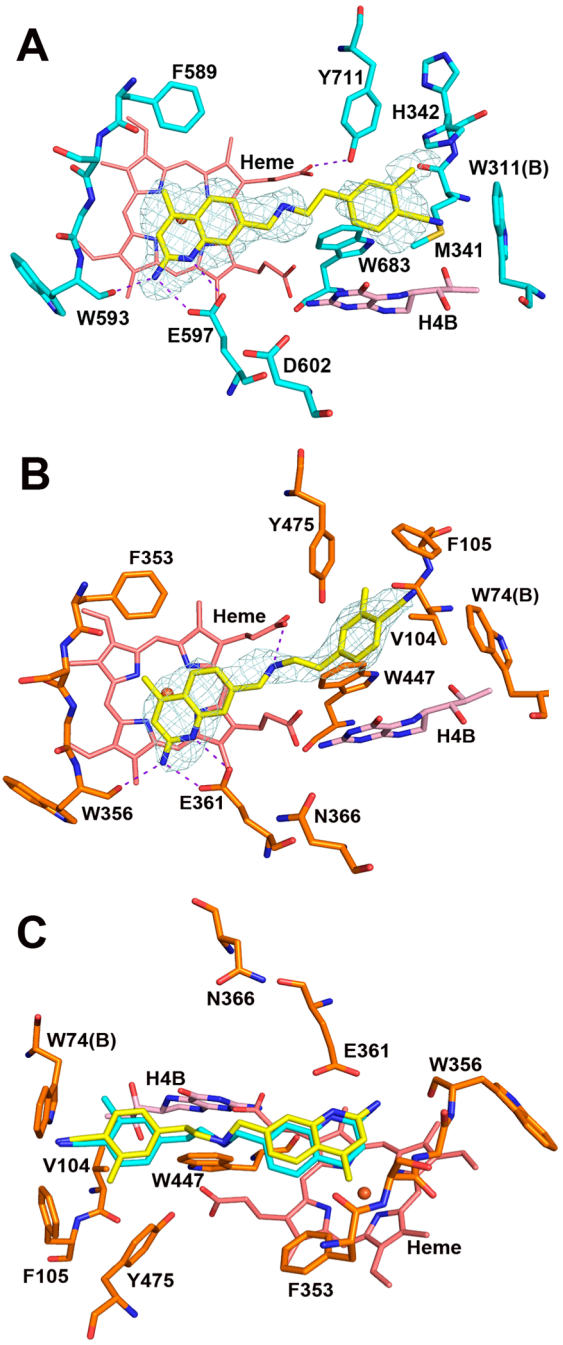

Figure 10. Active site structures of hnNOS-**25** (A) and heNOS-**25** (B). To illustrate the different binding modes of the 4-methylated vs unmethylated 2-aminoquinolines in heNOS, the structural model of **25** (yellow) is overlaid (C) with that of **22** (cyan). To better visualize the inhibitors, part C has been rotated relative to part B about an axis perpendicular to the figure plane by 180°.

argon. An Agilent 971-FP automated flash purification system with SiliaSep (Silicycle, 40–63 μm, 60 Å, 12–80 g) prepacked silica cartridges was used in purification of all compounds that required it. Melting points were determined in capillary tubes using a Buchi melting point B-540 apparatus and are uncorrected. ^{1}H and ^{13}C NMR spectra were determined using a Bruker Avance-III 500 (direct cryoprobe) instrument at 500 and 126 MHz, respectively. Low-resolution ESIMS was performed using a Bruker AmaZonSL ion trap mass spectrometer. High-resolution mass spectral data were obtained at the Integrated Molecular Structure Education and Research Center (Northwestern University) on an Agilent 6210A TOF mass

Table 3. PDSP Binding Summary for Selected Compounds[a]

compd	concerning	moderate	weak	insignificant	total
5	8	7	22	8	45
6	3	3	17	22	45
25	3	6	22	14	45

[a]Off-target binding is classified into four categories: *concerning* (K_i < 100 nM, or < ~2× nNOS K_i value), *moderate* (100–300 nM, or ~2–5× nNOS K_i value), *weak* (>300 nM, or > ~5× nNOS K_i value, typically ~1 μM), and *insignificant* (<50% bound at 10 μM), for a total of 45 receptors as assayed by the PDSP's "comprehensive screen" (see ref 17).

Table 4. Caco-2 Permeability Data for Selected Compounds[a]

	apparent permeability (P_{app}, 10^{-6} cm s^{-1})[b]			recovery (%)	
compd	mean A→B	mean B→A	efflux ratio[c]	A→B	B→A
5	30.3	24.5	0.81	98.0	67.0
25	20.8	20.1	0.97	58.5	83.0
warfarin[d]	23.2	22.5	0.97		
ranitidine[e]	0.15	1.2	8.0		
talinolol[f]	0.066	3.4	51.5		

[a]All assays were performed over 2 h at a concentration of 10 μM. See Experimental Section for details. [b]P_{app}: apparent permeability rate value. [c]Efflux ratio: P_{app} (B → A)/P_{app} (A → B). [d]High permeability control. [e]Low permeability control. [f]High efflux control.

spectrometer in positive ion mode using ESI, with an Agilent G1312A HPLC pump and an Agilent G1367B autoinjector. Data were processed using MassHunter software version B.02.00. Analytical HPLC was performed using an Agilent Infinity 1260 HPLC system with an injection volume of 10 μL. A Phenomenex Luna 5 μm C-8(2) 100 Å column, 50 mm × 4.60 mm, was used for all analytical HPLC experiments. The purity of all final target compounds was found to be ≥95% by HPLC, using a 10 min gradient of 95% H_2O/5% acetonitrile + 0.05% TFA to 95% acetonitrile/5% H_2O + 0.05% TFA, at 1.5 mL/min. Preparative HPLC was performed at the Center for Molecular Innovation and Drug Discovery ChemCore laboratory (Northwestern University), using an Agilent 1200 series HPLC, an Agilent 6120 quadrupole mass spectrometer (API-MS mode), and a Phenomenex Luna 5 μm C-8(2) 100 Å preparative HPLC column, 150 mm × 21.2 mm (gradients used are described under subheadings of individual compounds). Microwave chemistry was performed using a Biotage Initiator Sixty research microwave in Biotage vials. Analytical thin-layer chromatography was performed on Silicycle extra-hard 250 μm TLC plates. Intermediates and final analogues were visualized with short-wavelength UV light, $KMnO_4$, and ninhydrin stain, where relevant. Compounds **26**,[15] **42**,[29] **46–50**,[13,30,31] **52**,[37] **54**,[15] **75–77**,[33–35] and **85–90**[20,37] were prepared by known literature procedures, and their spectral data are consistent with those data reported for the same; their preparations are not reported here. The preparations of **43**, **44**, **53**, **64–69**, and **78–82** are described in the Supporting Information.

General Procedure 1: Synthesis and Deprotection of Truncated Aniline-Linked 2-Aminoquinolines.[26]

Step 1: A 5 mL sealable microwave vial was charged with intermediate **26** (1 equiv) and KI (10–15 mol %), which were then diluted with anhydrous MeCN (0.5–1 mL). A solution of the requisite aniline (3 equiv) in MeCN (1–1.5 mL) was added. The vial was sealed and the reaction stirred under microwave heating at 110 °C for 20–25 min. The resulting solution was diluted with CH_2Cl_2 (~20–30 mL) and washed with satd aq $NaHCO_3$ (3 × 20 mL). The aqueous phase was extracted with EtOAc (3 × 25 mL), and the combined organics were washed with H_2O (20 mL) and satd aq NaCl (20 mL), dried over anhydrous sodium sulfate, and concentrated. The residue was purified by flash column chromatography (SiO_2; the gradient is described below for individual compounds) to yield the desired

DOI: 10.1021/acs.jmedchem.7b00835
J. Med. Chem. XXXX, XXX, XXX–XXX

secondary amine. Step 2: The protected intermediate was immediately diluted with MeOH (9−10 mL) and K_2CO_3 (2 equiv) was added. The mixture was heated at reflux for 2−2.5 h, cooled, and concentrated, and the residue was partitioned between EtOAc (10 mL) and H_2O/satd aq NaCl (1:1, 10 mL). The layers were separated, the aqueous phase was extracted with EtOAc (3 × 20 mL), and the organics were combined, washed with satd aq NaCl (20 mL), dried over anhydrous sodium sulfate, and concentrated. Step 3: The resulting free 2-aminoquinoline was dissolved in MeOH (10 mL) and treated with methanolic HCl (~3 M, 1.5 mL). The mixture was stirred at room temperature for 20 min, and ether (15 mL) was added, which afforded the desired compound after filtration, washing with ether, and drying in vacuo.

*3-(((2-Aminoquinolin-7-yl)methyl)amino)benzonitrile Dihydrochloride (**7**).* Prepared from **26** (0.100 g, 0.36 mmol) and 3-aminobenzonitrile (**27**, 0.126 g, 1.07 mmol), using general procedure 1, step 1. After workup and purification by flash column chromatography, eluting with a gradient of 5% EtOAc in CH_2Cl_2 to 35% EtOAc in CH_2Cl_2, intermediate **32** (0.094 g, 88%) was deprotected with K_2CO_3 (0.082 g, 0.59 mmol), using general procedure 1, step 2. Following workup, the free aminoquinoline was converted to the dihydrochloride salt, following general procedure 1, step 3, to give the title compound as a white solid (0.093 g, 90% from **32**): mp 219−223 °C. ^{1}H NMR (500 MHz; DMSO-d_6): δ 14.07 (s, 1 H), 9.14 (br s, 1 H), 8.34 (d, J = 9.3 Hz, 1 H), 8.17 (br s, 1 H), 7.90 (d, J = 8.2 Hz, 1 H), 7.61 (br s, 1 H), 7.48 (dd, J = 8.2, 1.1 Hz, 1 H), 7.24 (t, J = 7.9 Hz, 1 H), 7.06 (d, J = 9.3 Hz, 1 H), 6.94−6.89 (m, 3 H), 4.53 (s, 2 H); the anilinium protons are broadened into residual water and appear as a broad hump at 5.78 ppm. ^{13}C NMR (126 MHz; DMSO-d_6): δ 154.5, 148.9, 145.5, 143.1, 136.1, 130.3, 129.1, 124.3, 120.0, 119.6, 119.5, 117.4, 114.7, 114.2, 113.3, 111.8, 45.8. ESIMS m/z (rel intensity) 275 (MH^+, 100). HRMS calcd for $C_{17}H_{15}N_4$, 275.1296; found, 275.1291.

*7-(((3-Fluorophenyl)amino)methyl)quinolin-2-amine Dihydrochloride (**8**).* Prepared from **26** (0.100 g, 0.36 mmol) and 3-fluoroaniline (**28**, 0.119 g, 1.07 mmol), using general procedure 1, step 1. After workup and purification by flash column chromatography, eluting with a gradient of 5% EtOAc in CH_2Cl_2 to 35% EtOAc in CH_2Cl_2, intermediate **33** (0.088 g, 84%) was deprotected with K_2CO_3 (0.078 g, 0.57 mmol), using general procedure 1, step 2. Following workup, the free aminoquinoline was converted to the dihydrochloride salt, following general procedure 1, step 3, to give the title compound as a white solid (0.084 g, 87% from **33**): mp 209−212 °C. ^{1}H NMR (500 MHz; DMSO-d_6): δ 14.09 (s, 1 H), 9.13 (br s, 1 H), 8.33 (d, J = 9.3 Hz, 1 H), 8.15 (br s, 1 H), 7.88 (d, J = 8.2 Hz, 1 H), 7.61 (s, 1 H), 7.47 (dd, J = 8.2, 0.9 Hz, 1 H), 7.07−7.02 (m, 2 H), 6.41 (dd, J = 8.2, 1.4 Hz, 1 H), 6.33−6.28 (m, 2 H), 4.47 (s, 2 H); the anilinium protons are broadened into residual water and appear as a broad hump at 5.65 ppm. ^{13}C NMR (126 MHz; DMSO-d_6): δ (164.5 + 162.6, 1 C), 154.5, (150.5 + 150.4, 1 C), 145.9, 143.1, 136.1, (130.53 + 130.45, 1 C), 129.0, 124.3, 120.0, 114.8, 113.3, 108.9, (102.4 + 102.2, 1 C), (98.8 + 98.6, 1 C), 46.2. ESIMS m/z (rel intensity) 268 (MH^+, 100). HRMS calcd for $C_{16}H_{15}FN_3$, 268.1250; found, 268.1244.

*7-(((3-Methoxyphenyl)amino)methyl)quinolin-2-amine Dihydrochloride (**9**).* Prepared from **26** (0.100 g, 0.36 mmol) and 3-methoxyaniline (**29**, 0.132g, 1.07 mmol), using general procedure 1, step 1. After workup and purification by flash column chromatography, eluting with a gradient of 5% EtOAc in CH_2Cl_2 to 35% EtOAc in CH_2Cl_2, intermediate **34** (0.082 g, 71%) was deprotected with K_2CO_3 (0.070 g, 0.51 mmol), using general procedure 1, step 2. Following workup, the free aminoquinoline was converted to the dihydrochloride salt, following general procedure 1, step 3, to give the title compound as a cream-colored solid (0.069 g, 77% from **34**): mp 237−240 °C. ^{1}H NMR (500 MHz; DMSO-d_6): δ 14.00 (s, 1 H), 9.09 (s, 1 H), 8.34 (d, J = 9.3 Hz, 1 H), 8.16 (s, 1 H), 7.88 (d, J = 8.2 Hz, 1 H), 7.63 (s, 1 H), 7.49 (dd, J = 8.2, 1.2 Hz, 1 H), 7.05 (d, J = 9.3 Hz, 1 H), 6.96 (t, J = 8.0 Hz, 1 H), 6.21−6.14 (m, 3 H), 4.46 (s, 2 H), 3.63 (s, 3 H); the anilinium protons are broadened into residual water and appear as a broad hump at 4.76 ppm. ^{13}C NMR (126 MHz; DMSO-d_6): δ 160.3, 154.2, 149.1, 146.1, 142.9, 135.9, 129.7, 128.8, 124.2, 119.8, 114.7, 113.1, 105.8, 101.9, 98.7, 54.6, 46.5. ESIMS m/z (rel intensity) 280 (MH^+, 40). HRMS calcd for $C_{17}H_{18}N_3O$, 280.1450; found, 280.1447.

*N-((2-Aminoquinolin-7-yl)methyl)-N,N-dimethylbenzene-1,3-diamine Trihydrochloride (**10**).* Prepared from **26** (0.100 g, 0.36 mmol) and *N*,*N*-dimethylbenzene-1,3-diamine (**30**, 0.225g, 1.07 mmol), using general procedure 1, step 1. After workup and purification by flash column chromatography, eluting with a gradient of 5% EtOAc in CH_2Cl_2 to 50% EtOAc in CH_2Cl_2, intermediate **35** (0.057 g, 48%) was deprotected with K_2CO_3 (0.047 g, 0.34 mmol), using general procedure 1, step 2. Following workup, the free aminoquinoline was converted to the trihydrochloride salt, following general procedure 1, step 3, to give the title compound as a white solid (0.043 g, 63% from **35**): mp 216−218 °C. ^{1}H NMR (500 MHz; DMSO-d_6): δ 14.16 (s, 1 H), 9.10 (s, 1 H), 8.34 (d, J = 9.0 Hz, 1 H), 8.16 (s, 1 H), 7.89 (d, J = 8.0 Hz, 1 H), 7.65 (s, 1 H), 7.49 (d, J = 8.0 Hz, 1 H), 7.17 (dd, J = 8.0, 8.0 Hz, 1 H), 7.06 (d, J = 9.0 Hz, 1 H), 6.90 (br s, 1 H), 6.81 (br s, 1 H), 6.57 (br s, 1 H), 4.50 (s, 2 H), 3.02 (s, 6 H); the anilinium protons are broadened into residual water and appear as a broad hump at 3.48 ppm. ^{13}C NMR (126 MHz; DMSO-d_6): δ 154.5, 149.5, 145.4, 143.3, 136.3, 130.9, 129.3, 124.9, 120.4, 115.5, 113.7, 113.0, 108.0, 104.6, 46.8, 45.7; one of the aminoquinoline carbons is not visible due to baseline broadening. ESIMS m/z (rel intensity) 293 (MH^+, 100). HRMS calcd for $C_{18}H_{21}N_4$, 293.1766; found, 293.1759.

*N-((2-Aminoquinolin-7-yl)methyl)-N,N-dimethylbenzene-1,4-diamine Trihydrochloride (**11**).* Prepared from **26** (0.056 g, 0.20 mmol) and *N*,*N*-dimethylbenzene-1,4-diamine (**31**, 0.127g, 0.60 mmol), using general procedure 1, step 1. After workup and purification by flash column chromatography, eluting with a gradient of 5% EtOAc in CH_2Cl_2 to 50% EtOAc in CH_2Cl_2, intermediate **36** (0.052 g, 77%) was deprotected with K_2CO_3 (0.044 g, 0.32 mmol), using general procedure 1, step 2. Following workup and purification by flash column chromatography, eluting with a gradient of EtOAc to 15% MeOH in EtOAc, the free aminoquinoline was converted to the trihydrochloride salt, following general procedure 1, step 3, to give the title compound as an off-white solid (0.027 g, 41% from **36**): mp 242−244 °C. ^{1}H NMR (500 MHz; DMSO-d_6): δ 14.02 (s, 1 H), 12.36 (s, 1 H), 9.09 (s, 1 H), 8.33 (d, J = 9.0 Hz, 1 H), 8.13 (s, 1 H), 7.88 (d, J = 8.0 Hz, 1 H), 7.60 (s, 1 H), 7.47 (d, J = 8.0 Hz, 1 H), 7.43 (d, J = 6.0 Hz, 2 H), 7.03 (d, J = 9.0 Hz, 1 H), 6.64 (d, J = 6.0 Hz, 2 H), 4.50 (s, 2 H), 3.01 (s, 6 H); the anilinium protons are broadened into residual water and appear as a broad hump at 4.09 ppm. ^{13}C NMR (126 MHz; DMSO-d_6): δ 154.9, 149.3, 146.1, 143.3, 136.3, 129.4, 124.6, 122.1, 120.4, 115.1, 113.7, 112.8, 46.3; the methyl carbon signal overlaps with the solvent signal, and one of the aminoquinoline carbons is not visible due to baseline broadening. ESIMS m/z (rel intensity) 293 (MH^+, 100). HRMS calcd for $C_{18}H_{21}N_4$, 293.1766; found, 293.1764.

*7-(((3-(Dimethylamino)benzyl)amino)methyl)quinolin-2-amine Trihydrochloride (**12**).* [25]

3-(Aminomethyl)-*N*,*N*-dimethylaniline (**37**, 0.044 g, 0.29 mmol) and Cs_2CO_3 (0.094 g, 0.29 mmol) were diluted with anhydrous DMF (3 mL) and stirred for 30 min at room temperature. A solution of **26** (0.070 g, 0.25 mmol) in anhydrous DMF (1 mL) was added dropwise over 5 min while stirring, and the resulting yellow solution was stirred at room temperature for 16 h and concentrated. The residue was diluted with EtOAc (50 mL) and washed with H_2O (2 × 50 mL) and satd aq NaCl (50 mL). The organics were dried with anhydrous sodium sulfate, concentrated, and diluted with anhydrous THF (5 mL). A solution of Boc_2O (0.073 g, 0.34 mmol) in anhydrous THF (2 mL) was added dropwise, and the mixture was stirred at room temperature for 18 h. The mixture was concentrated, diluted with CH_2Cl_2 (25 mL), and washed with satd aq $NaHCO_3$ (30 mL), H_2O (30 mL), and satd aq NaCl (30 mL). The organic layer was dried over anhydrous sodium sulfate, concentrated, and purified by flash column chromatography, eluting with a gradient of CH_2Cl_2 to 40% EtOAc in CH_2Cl_2 to afford **39** as a clear oil (0.050 g, 45%). This was deprotected using K_2CO_3 (0.031 g, 0.22 mmol), using general procedure 1, step 2. After workup, the resulting clear oil was treated with methanolic HCl (3 mL), the mixture was stirred at room temperature for 16 h, and ether (15 mL) was added, affording an off-white solid (0.030 g, 65% from **39**) after filtration and washing with

DOI: 10.1021/acs.jmedchem.7b00835
J. Med. Chem. XXXX, XXX, XXX−XXX

ether: mp 294−295 °C. ^{1}H NMR (500 MHz; DMSO-d_6): δ 14.61 (s, 1 H), 10.08 (s, 2 H), 9.39 (br s, 1 H), 8.39 (d, J = 9.5 Hz, 1 H), 8.36 (br s, 1 H), 7.97 (d, J = 8.5 Hz, 1 H), 7.87 (s, 1 H), 7.71 (d, J = 8.5 Hz, 1 H), 7.49−7.31 (m, 2 H), 7.18 (d, J = 9.5 Hz, 1 H), 7.11 (br s, 2 H), 4.32 (t, J = 5.0 Hz, 2 H), 4.16 (t, J = 5.0 Hz, 2 H), 2.99 (s, 6 H); the anilinium proton is broadened into residual water and appears as a broad hump at 4.90 ppm. ^{13}C NMR (126 MHz; DMSO-d_6): δ 155.2, 143.1, 137.0, 135.8, 133.4, 130.0, 129.4, 127.2, 121.3, 119.3, 117.2, 115.0, 50.6, 49.8, 42.7; one of the aminoquinoline carbons and two of the aryl carbons are not visible due to baseline broadening. ESIMS m/z (rel intensity) 307 (MH^+, 100). HRMS calcd for $C_{19}H_{23}N_4$, 307.1923; found, 307.1915.

*7-(((4-(Dimethylamino)benzyl)amino)methyl)quinolin-2-amine Trihydrochloride (**13**).* [25]

4-(Aminomethyl)-*N*,*N*-dimethylaniline dihydrochloride (**38**, 0.041 g, 0.41 mmol) and Cs_2CO_3 (0.370 g, 1.13 mmol) were diluted with anhydrous DMF (3.5 mL) and stirred for 30 min at room temperature. A solution of **26** (0.100 g, 0.36 mmol) in anhydrous DMF (1 mL) was added dropwise over 5 min while stirring. The resulting pale-yellow solution was stirred at room temperature for 16 h and concentrated. The residue was diluted with EtOAc (50 mL) and washed with H_2O (2 × 50 mL) and satd aq NaCl (50 mL). The organic layer was dried over anhydrous sodium sulfate, concentrated, and diluted with anhydrous THF (5 mL). A solution of Boc_2O (0.103 g, 0.47 mmol) in anhydrous THF (3 mL) was added dropwise, and the mixture was stirred at room temperature for 18 h. The mixture was concentrated, diluted with CH_2Cl_2 (25 mL), and washed with satd aq $NaHCO_3$ (30 mL), H_2O (30 mL), and satd aq NaCl (30 mL). The organic layer was dried over anhydrous sodium sulfate, concentrated, and purified by flash column chromatography, eluting with a gradient of CH_2Cl_2 to 40% EtOAc in CH_2Cl_2 to afford **40** as a clear oil (0.071 g, 37%). This was deprotected using K_2CO_3 (0.031 g, 0.22 mmol), using general procedure 1, step 2. After workup, the resulting clear oil was treated with methanolic HCl (3 mL), the mixture was stirred at room temperature for 16 h and ether (15 mL) was added, affording a white solid (0.042 g, 64% from **40**) after filtration and washing with ether: mp 366−368 °C. ^{1}H NMR (500 MHz; DMSO-d_6): δ 14.65 (s, 1 H), 10.01 (s, 2 H), 9.43 (s, 1 H), 8.38 (d, J = 9.0 Hz, 1 H), 8.36 (br s, 1 H), 7.95 (d, J = 8.5 Hz, 1 H), 7.85 (s, 1 H), 7.70 (d, J = 8.5 Hz, 1 H), 7.57 (br s, 2 H), 7.24 (br s, 2 H), 7.18 (d, J = 9.0 Hz, 1 H), 4.28 (t, J = 5.5 Hz, 2 H), 4.13 (t, J = 5.5 Hz, 2 H), 3.00 (s, 6 H); the anilinium proton is broadened into residual water and appears as a broad hump at 4.62 ppm. ^{13}C NMR (126 MHz; DMSO-d_6): δ 155.2, 148.0, 143.1, 137.1, 135.7, 132.0, 129.4, 127.1, 121.3, 119.2, 116.5, 114.9, 50.0, 49.6, 42.9; one of the aminoquinoline carbons is not visible due to baseline broadening. ESIMS m/z (rel intensity) 307 (MH^+, 100). HRMS calcd for $C_{19}H_{23}N_4$, 307.1923; found, 307.1914.

General Procedure 2: Synthesis of 2-Aminoquinolines Containing a Phenethylamine or Phenylpropylamine-Derived Tail Portion. Step 1: The requisite phenethylamine or propylamine (1.1−1.2 equiv) was diluted with anhydrous $CHCl_3$ (6−9 mL) or $CHCl_3$/MeOH (10:1−5:1). If the amine was a hydrochloride salt, Et_3N (1.5−2 equiv) was added and the mixture was stirred until clear. Aldehyde **54** or **90** (1 equiv, as a solution in minimal $CHCl_3$) and anhydrous sodium sulfate (~1 g) were added to the reaction mixture, and the resulting suspension was stirred at room temperature for 1 h. Acetic acid (10 μL/10 mg amine) was added, and the mixture was stirred at room temperature for 16 h. The resulting solution was filtered and concentrated to give the crude imine, which was diluted with MeOH (4−7 mL) and cooled to 0 °C. $NaBH_4$ (1.5 equiv) was added while stirring, and the mixture was warmed to room temperature, stirred for 20 min, and concentrated. The residue was diluted with EtOAc (30 mL) and washed with satd aq $NaHCO_3$ (25 mL), H_2O (25 mL), and satd aq NaCl (25 mL). The organic layer was dried over anhydrous sodium sulfate and concentrated. Step 2: The crude amine was diluted with anhydrous THF (5−7 mL) and Boc_2O (1.1−1.2 equiv, as a solution in minimal anhydrous THF) was added. The mixture was stirred at room temperature for 4−18 h and concentrated, and the residue was purified by flash column chromatography (SiO_2; the gradient is described below for individual compounds) to yield the Boc-protected amine. Step 3: This intermediate was not characterized but was instead deprotected as in general procedure 1, step 2. Step 4: After workup, the resulting unprotected aminoquinoline was treated with methanolic HCl (1.5 mL) in ether (5−10 mL), and the mixture was stirred at room temperature for 16 h. Ether (15−20 mL) was then added, which afforded the desired compound after filtration and washing with ether. If one ether wash was insufficient to remove impurities, compounds were precipitated from methanol (1 mL) with ether (15 mL), washed with ether, and dried in vacuo.

*3-(Dimethylamino)phenethyl)amino)methyl)quinolin-2-amine Trihydrochloride (**14**).* Prepared from aldehyde **54** (0.080 g, 0.37 mmol) and phenethylamine **44** (0.073 g, 0.44 mmol), using general procedure 2, step 1. After concentration, reduction with $NaBH_4$ (0.021 g, 0.55 mmol), and workup, the secondary amine was protected with Boc_2O (0.089 g, 0.41 mmol), following general procedure 2, step 2. Workup and purification by flash column chromatography, eluting with a gradient of CH_2Cl_2 to 15% EtOAc in CH_2Cl_2, afforded the protected intermediate **56** (0.153 g, 90%). This was immediately deprotected with K_2CO_3 (0.091 g, 0.66 mmol) following general procedure 2, step 3. Following workup, the Boc group was removed, following general procedure 2, step 4. An analytically pure sample for assay was prepared by preparative LC-MS, using the instrument and column detailed in the General Procedures section, eluting with a gradient of H_2O + 0.1% formic acid to 10% MeOH + 0.1% formic acid/90% H_2O + 0.1% formic acid. The purified compound was converted to the trihydrochloride salt following general procedure 1, step 3, to give the title compound as an off-white solid (0.016 g, 10% from **56**): mp 276−278 °C. ^{1}H NMR (500 MHz; DMSO-d_6): δ 14.50 (s, 1 H), 9.68 (s, 2 H), 9.31 (br s, 1 H), 8.39 (d, J = 9.0 Hz, 1 H), 8.28 (br s, 1 H), 7.99 (d, J = 8.0 Hz, 1 H), 7.88 (s, 1 H), 7.69 (d, J = 8.0 Hz, 1 H), 7.27 (br s, 1 H), 7.16 (d, J = 9.0 Hz, 1 H), 6.86 (br s, 3 H), 4.36 (t, J = 6.0 Hz, 2 H), 3.22−3.16 (m, 2 H), 3.01−2.90 (m, 8 H); the anilinium proton is broadened into residual water and appears as a broad hump at 4.41 ppm. ^{13}C NMR (126 MHz; DMSO-d_6): δ 155.4, 143.2, 139.0, 137.1, 135.9, 130.2, 129.6, 127.0, 121.4, 119.2, 115.0, 49.9, 48.0, 32.1; four of the aryl carbons are not visible due to baseline broadening and the methyl carbon signal overlaps with the solvent signal. ESIMS m/z (rel intensity) 321 (MH^+, 100). HRMS calcd for $C_{20}H_{25}N_4$, 321.2079; found, 321.2072.

*7-(((4-(Dimethylamino)phenethyl)amino)methyl)quinolin-2-amine Trihydrochloride (**15**).* Prepared from aldehyde **54** (0.080 g, 0.37 mmol) and phenethylamine **47** (0.073 g, 0.44 mmol), using general procedure 2, step 1. After concentration, reduction with $NaBH_4$ (0.021 g, 0.55 mmol), and workup, the secondary amine was protected with Boc_2O (0.089 g, 0.41 mmol), following general procedure 2, step 2. Workup and purification by flash column chromatography, eluting with a gradient of CH_2Cl_2 to 15% EtOAc in CH_2Cl_2, afforded the protected intermediate **57** (0.069 g, 40%). This was immediately deprotected with K_2CO_3 (0.041 g, 0.30 mmol) following general procedure 2, step 3. Following workup, the Boc group was removed using general procedure 2, step 4. An analytically pure sample for assay was prepared by preparative LC-MS, using the instrument and column detailed in the General Procedures section, eluting with a gradient of H_2O + 0.1% formic acid to 20% MeOH + 0.1% formic acid/80% H_2O + 0.1% formic acid. The purified compound was converted to the trihydrochloride salt following general procedure 1, step 3, to give the title compound as a white solid (0.008 g, 13% from **57**): mp 243−245 °C. ^{1}H NMR (500 MHz; DMSO-d_6): δ 14.37 (s, 1 H), 9.48 (s, 2 H), 9.24 (s, 1 H), 8.39 (d, J = 9.0 Hz, 1 H), 8.25 (s, 1 H), 7.99 (d, J = 8.0 Hz, 1 H), 7.85 (s, 1 H), 7.65 (d, J = 8.0 Hz, 1 H), 7.54 (d, J = 9.0 Hz, 1 H), 6.84 (br s, 4 H), 4.35 (t, J = 5.5 Hz, 2 H), 3.12 (br s, 2 H), 2.92 (br s, 8 H); the anilinium proton is broadened into residual water and appears as a broad hump at 3.81 ppm. ^{13}C NMR (126 MHz; DMSO-d_6): δ 155.1, 143.2, 137.0, 135.9, 129.8, 129.6, 127.0, 126.9, 121.4, 119.2, 115.0, 49.9, 48.5, 31.1, 29.0; two of the aminoquinoline carbons are not visible due to baseline broadening. ESIMS m/z (rel intensity) 321 (MH^+, 100). HRMS calcd for $C_{20}H_{25}N_4$, 321.2079; found, 321.2071.

DOI: 10.1021/acs.jmedchem.7b00835
J. Med. Chem. XXXX, XXX, XXX−XXX

*7-(((3-(Pyridin-3-yl)propyl)amino)methyl)quinolin-2-amine Trihydrochloride (**16**).* Prepared from aldehyde **54** (0.080 g, 0.37 mmol) and phenpropylamine **50** (0.086 g, 0.41 mmol), using general procedure 2, step 1. After concentration, reduction with $NaBH_4$ (0.021 g, 0.55 mmol), and workup, the secondary amine was protected with Boc_2O (0.088 g, 0.40 mmol), following general procedure 2, step 2. Workup and purification by flash column chromatography, eluting with a gradient of EtOAc to 5% MeOH in EtOAc, afforded the protected intermediate **58** (0.110 g, 68%). This was immediately deprotected with K_2CO_3 (0.070 g, 0.51 mmol) following general procedure 2, step 3. Following workup, the Boc group was removed using general procedure 2, step 4, to give the title compound as a white solid (0.075 g, 74% from **58**): mp: 260−262.5 °C. ^{1}H NMR (500 MHz; DMSO-d_6): δ 14.57 (br s, 1 H), 9.72 (s, 2 H), 9.33 (br s, 1 H), 8.82 (s, 1 H), 8.74 (d, J = 4.7 Hz, 1 H), 8.40−8.34 (m, 3 H), 7.98 (d, J = 8.2 Hz, 1 H), 7.91−7.88 (m, 2 H), 7.71 (dd, J = 8.2, 1.4 Hz, 1 H), 7.16 (d, J = 9.3 Hz, 1 H), 4.31 (t, J = 5.6 Hz, 2 H), 2.98−2.93 (m, 2 H), 2.89 (t, J = 7.6 Hz, 2 H), 2.09 (quintet, J = 7.5 Hz, 2 H); the pyridinium proton is broadened into residual water and appears as a broad hump at 4.52 ppm. ^{13}C NMR (126 MHz; DMSO-d_6): δ 154.8, 144.0, 143.2, 142.9, 141.6, 139.9, 136.8, 135.5, 129.2, 126.7, 126.4, 121.0, 118.9, 114.7, 49.5, 45.8, 28.8, 26.3. ESIMS m/z (rel intensity) 293 (MH^+, 100). HRMS calcd for $C_{18}H_{21}N_4$, 293.1766; found, 293.1759.

*7-(((3-(4-Methylpyridin-3-yl)propyl)amino)methyl)quinolin-2-amine Trihydrochloride (**17**).* Prepared from aldehyde **54** (0.080 g, 0.37 mmol) and phenpropylamine **67** (0.092 g, 0.41 mmol), using general procedure 2, step 1. After concentration, reduction with $NaBH_4$ (0.021 g, 0.55 mmol), and workup, the secondary amine was protected with Boc_2O (0.088 g, 0.40 mmol), following general procedure 2, step 2. Workup and purification by flash column chromatography, eluting with a gradient of EtOAc to 5% MeOH in EtOAc, afforded the protected intermediate **70** (0.118 g, 71%). This was immediately deprotected with K_2CO_3 (0.072 g, 0.53 mmol) following general procedure 2, step 3. Following workup, the Boc group was removed using general procedure 2, step 4, to give the title compound as a white solid (0.075 g, 69% from **70**) after precipitation from hot MeOH (1 mL) using ether (15 mL): mp: 287−290 °C. ^{1}H NMR (500 MHz; DMSO-d_6): δ 14.73 (br s, 1 H), 9.81 (s, 2 H), 9.34 (br s, 1 H), 8.74 (s, 1 H), 8.67 (d, J = 5.9 Hz, 1 H), 8.39 (d, J = 9.3 Hz, 1 H), 8.30 (br s, 1 H), 7.98 (d, J = 8.2 Hz, 1 H), 7.88 (s, 1 H), 7.86 (d, J = 5.8 Hz, 1 H), 7.74 (dd, J = 8.2, 1.4 Hz, 1 H), 7.17 (d, J = 9.3 Hz, 1 H), 4.32 (t, J = 5.4 Hz, 2 H), 3.01−2.98 (m, 2 H), 2.89 (t, J = 7.8 Hz, 2 H), 2.55−2.53 (m, 3 H), 2.08−2.02 (m, 2 H); the pyridinium proton is broadened into residual water and appears as a broad hump at 3.65 ppm. ^{13}C NMR (126 MHz; DMSO-d_6): δ 154.7, 142.7, 140.5, 139.41, 139.40, 138.9, 136.7, 135.4, 129.1, 127.8, 126.6, 120.9, 118.7, 114.5, 49.4, 45.9, 26.5, 24.6, 19.5. ESIMS m/z (rel intensity) 307 (MH^+, 100). HRMS calcd for $C_{19}H_{23}N_4$, 307.1923; found, 307.1923.

*7-(((3-(4-Methoxypyridin-3-yl)propyl)amino)methyl)quinolin-2-amine Trihydrochloride (**18**).* Prepared from aldehyde **54** (0.080 g, 0.37 mmol) and phenpropylamine **68** (0.107 g, 0.45 mmol), using general procedure 2, step 1. After concentration, reduction with $NaBH_4$ (0.021 g, 0.55 mmol), and workup, the secondary amine was protected with Boc_2O (0.098 g, 0.45 mmol), following general procedure 2, step 2. Workup and purification by flash column chromatography, eluting with a gradient of EtOAc to 7% MeOH in EtOAc, afforded the protected intermediate **71** (0.133 g, 77%). This was immediately deprotected with K_2CO_3 (0.072 g, 0.53 mmol) following general procedure 2, step 3. Following workup, the Boc group was removed using general procedure 2, step 4, to give the title compound as a white solid (0.100 g, 81% from **71**) after precipitation from hot MeOH (1 mL) using ether (15 mL): mp: 225−228 °C. ^{1}H NMR (500 MHz; DMSO-d_6): δ 9.63 (br s, 2 H), 8.77 (d, J = 6.7 Hz, 1 H), 8.68 (s, 1 H), 8.39 (d, J = 9.4 Hz, 1 H), 7.98 (d, J = 8.2 Hz, 1 H), 7.87 (s, 1 H), 7.69 (dd, J = 8.2, 1.4 Hz, 1 H), 7.61 (d, J = 6.8 Hz, 1 H), 7.15 (d, J = 9.3 Hz, 1 H), 4.32−4.30 (m, 2 H), 4.11 (s, 3 H), 2.98−2.93 (m, 2 H), 2.76 (t, J = 7.5 Hz, 2 H), 2.04−1.98 (m, 2 H). The pyridinium, quinolinium, and aminoquinoline N−H protons are broadened into residual water and appear as a broad hump at 3.39 ppm. ^{13}C NMR (126 MHz; DMSO-d_6): δ 154.9, 143.1, 142.8, 141.3, 136.7, 135.7, 129.2, 127.8, 126.7, 121.1, 118.9, 114.7, 109.3, 58.0, 49.6, 46.0, 24.3, 23.9; one of the aryl carbons is not visible due to baseline broadening. ESIMS m/z (rel intensity) 323 (MH^+, 100). HRMS calcd for $C_{19}H_{23}N_4O$, 323.1872; found, 323.1867.

*7-(((3-(5-Fluoropyridin-3-yl)propyl)amino)methyl)quinolin-2-amine Trihydrochloride (**19**).* Prepared from aldehyde **54** (0.065 g, 0.30 mmol) and phenpropylamine **69** (0.082 g, 0.36 mmol), using general procedure 2, step 1. After concentration, reduction with $NaBH_4$ (0.017 g, 0.45 mmol), and workup, the secondary amine was protected with Boc_2O (0.072 g, 0.33 mmol), following general procedure 2, step 2. Workup and purification by flash column chromatography, eluting with EtOAc, afforded the protected intermediate **72** (0.108 g, 79%). This was immediately deprotected with K_2CO_3 (0.066 g, 0.48 mmol) following general procedure 2, step 3. Following workup, the Boc group was removed using general procedure 2, step 4, to give the title compound as a white solid (0.039 g, 40% from **72**): mp 236−237 °C. ^{1}H NMR (500 MHz; DMSO-d_6): δ 14.60 (s, 1 H), 9.80 (s, 2 H), 9.43 (s, 1 H), 8.57 (s, 1 H), 8.46 (s, 1 H), 8.38 (d, J = 9.5 Hz, 1 H), 8.35 (br s, 1 H), 7.96 (d, J = 8.0 Hz, 1 H), 7.87 (s, 1 H), 7.85 (s, 1 H), 7.73 (d, J = 8.0 Hz, 1 H), 7.19 (d, J = 9.5 Hz, 1 H), 4.30 (t, J = 5.5 Hz, 2 H), 2.97−2.87 (m, 2 H), 2.80 (t, J = 7.5 Hz, 2 H), 2.10−2.04 (m, 2 H); the pyridinium proton is broadened into residual water and appears as a broad hump at 5.29 ppm. ^{13}C NMR (126 MHz; DMSO-d_6): δ (160.7 + 158.7, 1 C), 155.2, 144.9, 143.1, 140.0, 137.2, 135.8, (134.8 + 134.6, 1 C), 129.5, 127.0, (125.4 + 125.3, 1 C), 121.3, 119.1, 115.0, 49.8, 46.2, 28.9, 26.7. ESIMS m/z (rel intensity) 311 (MH^+, 100). HRMS calcd for $C_{18}H_{20}FN_4$, 311.1672; found, 311.1669.

*3-(2-(((2-Aminoquinolin-7-yl)methyl)amino)ethyl)benzonitrile Dihydrochloride (**20**).* Prepared from aldehyde **54** (0.065 g, 0.30 mmol) and phenethylamine **53** (0.061 g, 0.33 mmol), using general procedure 2, step 1. After concentration, reduction with $NaBH_4$ (0.016 g, 0.42 mmol), and workup, the secondary amine was protected with Boc_2O (0.072 g, 0.33 mmol), following general procedure 2, step 2. Workup and purification by flash column chromatography, eluting with a gradient of 5% EtOAc in CH_2Cl_2 to 30% EtOAc in CH_2Cl_2, afforded the protected intermediate **59** (0.120 g, 89%). This was immediately deprotected with K_2CO_3 (0.078 g, 0.54 mmol) following general procedure 2, step 3. Following workup and purification by flash column chromatography, eluting with a gradient of EtOAc to 5% MeOH in EtOAc, the Boc group was removed using general procedure 2, step 4, to give the title compound as a white solid (0.076 g, 75% from **59**): mp 268−269 °C (softens), 290−293 °C (melts). ^{1}H NMR (500 MHz; DMSO-d_6): δ 14.52 (s, 1 H), 9.72 (s, 2 H), 9.31 (br s, 1 H), 8.38 (d, J = 9.3 Hz, 1 H), 8.30 (br s, 1 H), 7.97 (d, J = 8.2 Hz, 1 H), 7.87 (s, 1 H), 7.78 (s, 1 H), 7.74 (dt, J = 7.7, 1.3 Hz, 1 H), 7.68 (dd, J = 8.2, 1.0 Hz, 1 H), 7.64 (d, J = 8.0 Hz, 1 H), 7.56 (t, J = 7.7 Hz, 1 H), 7.15 (d, J = 9.3 Hz, 1 H), 4.34 (s, 2 H), 3.24−3.23 (m, 2 H), 3.11 (t, J = 7.9 Hz, 2 H). ^{13}C NMR (126 MHz; DMSO-d_6): δ 154.7, 142.6, 138.9, 136.4, 133.9, 132.3, 130.7, 129.8, 129.1, 126.5, 120.9, 118.8, 118.7, 114.5, 111.5, 49.5, 47.1, 30.8; one of the quinoline carbons is not visible due to baseline broadening. ESIMS m/z (rel intensity) 303 (MH^+, 100). HRMS calcd for $C_{19}H_{19}N_4$, 303.1610; found, 303.1602.

*4-(2-(((2-Aminoquinolin-7-yl)methyl)amino)ethyl)benzonitrile Dihydrochloride (**21**).* Prepared from aldehyde **54** (0.070 g, 0.33 mmol) and 4-cyano-phenethylamine hydrochloride (**55**, 0.071 g, 0.39 mmol), using general procedure 2, step 1. After concentration, reduction with $NaBH_4$ (0.019 g, 0.50 mmol), and workup, the secondary amine was protected with Boc_2O (0.078 g, 0.36 mmol), following general procedure 2, step 2. Workup and purification by flash column chromatography, eluting with a gradient of CH_2Cl_2 to 10% EtOAc in CH_2Cl_2, afforded the protected intermediate **60** (0.118 g, 79%). This was immediately deprotected with K_2CO_3 (0.072 g, 0.52 mmol) following general procedure 2, step 3. Following workup, the Boc group was removed using general procedure 2, step 4, to give the title compound as a white solid (0.057 g, 57% from **60**): mp 292−294 °C. ^{1}H NMR (500 MHz; DMSO-d_6): δ 14.57 (s, 1 H), 9.85 (s, 2 H), 9.36 (s, 1 H), 8.38 (d, J = 9.5 Hz, 1 H), 8.33 (br s, 1 H), 7.97 (d, J =

DOI: 10.1021/acs.jmedchem.7b00835
J. Med. Chem. XXXX, XXX, XXX−XXX

8.0 Hz, 1 H), 7.87 (s, 1 H), 7.81 (d, J = 8.0 Hz, 2 H), 7.71 (d, J = 9.5 Hz, 1 H), 7.49 (d, J = 8.0 Hz, 2 H), 7.17 (d, J = 8.0 Hz, 1 H), 4.34 (s, 2 H), 3.21 (t, J = 5.0 Hz, 2 H), 3.18−3.12 (m, 2 H). ^{13}C NMR (126 MHz, DMSO-d_6): δ 159.9, 148.5, 147.9, 147.8, 141.7, 140.7, 137.8, 135.0, 134.3, 131.8, 126.1, 124.0, 119.7, 114.9, 54.7, 52.2, 36.6. ESIMS m/z (rel intensity) 303 (MH^+, 100). HRMS calcd for $C_{19}H_{19}N_4$, 303.1610; found, 303.1603.

*4-(2-(((2-Aminoquinolin-7-yl)methyl)amino)ethyl)-2-methylbenzonitrile Dihydrochloride (**22**).* Prepared from aldehyde **54** (0.037 g, 0.17 mmol) and phenethylamine **81** (0.040 g, 0.20 mmol), using general procedure 2, step 1. After concentration, reduction with $NaBH_4$ (0.010 g, 0.26 mmol), and workup, the secondary amine was protected with Boc_2O (0.041 g, 0.19 mmol), following general procedure 2, step 2. Workup and purification by flash column chromatography, eluting with a gradient of CH_2Cl_2 to 15% EtOAc in CH_2Cl_2, afforded the protected intermediate **83** (0.043 g, 55%). This was immediately deprotected with K_2CO_3 (0.026 g, 0.19 mmol) following general procedure 2, step 3. Following workup, the Boc group was removed using general procedure 2, step 4, to give the title compound as a white solid (0.019 g, 54% from **83**): mp 316−317 °C. ^{1}H NMR (500 MHz; DMSO-d_6): δ 14.43 (s, 1 H), 9.65 (s, 2 H), 9.24 (s, 1 H), 8.38 (d, J = 9.0 Hz, 1 H), 8.28 (br s, 1 H), 7.98 (d, J = 8.0 Hz, 1 H), 7.86 (s, 1 H), 7.74 (d, J = 8.0 Hz, 1 H), 7.65 (d, J = 8.0 Hz, 1 H), 7.37 (s, 1 H), 7.29 (d, J = 8.0 Hz, 1 H), 7.14 (d, J = 9.0 Hz, 1 H), 4.35 (s, 2 H), 3.26−3.17 (m, 2 H), 3.12−3.08 (m, 2 H), 2.47 (s, 3 H). ^{13}C NMR (126 MHz; DMSO-d_6): δ 154.6, 152.5, 143.7, 137.7, 135.8, 133.0, 130.3, 126.8, 121.7, 119.6, 119.3, 113.7, 110.2, 49.8, 47.4, 31.9, 19.5; three of the aminoquinoline carbons are not visible due to baseline broadening. ESIMS m/z (rel intensity) 317 (MH^+, 100). HRMS calcd for $C_{20}H_{21}N_4$, 317.1766; found, 317.1759.

*4-(2-(((2-Aminoquinolin-7-yl)methyl)amino)ethyl)-2-chlorobenzonitrile Dihydrochloride (**23**).* Prepared from aldehyde **54** (0.029 g, 0.13 mmol) and phenethylamine **82** (0.035 g, 0.16 mmol), using general procedure 2, step 1. After concentration, reduction with $NaBH_4$ (0.008 g, 0.20 mmol), and workup, the secondary amine was protected with Boc_2O (0.031 g, 0.14 mmol), following general procedure 2, step 2. Workup and purification by flash column chromatography, eluting with a gradient of 5% EtOAc in CH_2Cl_2 to 35% EtOAc in CH_2Cl_2, afforded the protected intermediate **84** (0.046 g, 72%). This was immediately deprotected with K_2CO_3 (0.027 g, 0.19 mmol) following general procedure 2, step 3. Following workup, the Boc group was removed using general procedure 2, step 4, to give the title compound as a cream-colored solid (0.022 g, 56% from **84**): mp 309−311 °C. ^{1}H NMR (500 MHz; DMSO-d_6): δ 14.37 (s, 1 H), 9.58 (s, 2 H), 9.24 (br s, 1 H), 8.38 (d, J = 8.0 Hz, 1 H), 8.24 (br s, 1 H), 8.02−7.94 (m, 2 H), 7.85 (s, 1 H), 7.77 (s, 1 H), 7.64 (d, J = 8.0 Hz, 1 H), 7.49 (dd, J = 9.0 Hz, 1.5 Hz, 1 H), 7.14 (d, J = 9.0 Hz, 1 H), 4.39−4.32 (m, 2 H), 3.28 (s, 2 H), 3.17−3.12 (m, 2 H). ^{13}C NMR (126 MHz; DMSO-d_6): δ 155.1, 145.9, 143.2, 135.9, 135.2, 130.8, 129.6, 129.2, 126.9, 121.5, 119.3, 116.5, 115.0, 110.8, 60.1, 47.1, 31.6; two of the aminoquinoline carbons are not visible due to baseline broadening. ESIMS m/z (rel intensity) 337/339 (MH^+, 100/35). HRMS calcd for $C_{19}H_{18}ClN_4$, 337.1220; found, 337.1218.

*4-(2-(((2-Amino-4-methylquinolin-7-yl)methyl)amino)ethyl)-benzonitrile Dihydrochloride (**24**).* Prepared from aldehyde **90** (0.060 g, 0.26 mmol) and 4-cyanophenethylamine hydrochloride (**55**, 0.058 g, 0.32 mmol), using general procedure 2, step 1. After concentration, reduction with $NaBH_4$ (0.015 g, 0.39 mmol), and workup, the secondary amine was protected with Boc_2O (0.063 g, 0.29 mmol), following general procedure 2, step 2. Workup and purification by flash column chromatography, eluting with a gradient of CH_2Cl_2 to 12% EtOAc in CH_2Cl_2, afforded the protected intermediate **91** (0.071 g, 62%). This was immediately deprotected with K_2CO_3 (0.044 g, 0.32 mmol) following general procedure 2, step 3. Following workup, the Boc group was removed using general procedure 2, step 4, to give the title compound as a white solid (0.029 g, 47% from **91**): mp 304−306 °C. ^{1}H NMR (500 MHz; DMSO-d_6): δ 14.28 (s, 1 H), 9.73 (s, 2 H), 9.11 (br s, 1 H), 8.18 (br s, 1 H), 8.05 (d, J = 8.0 Hz, 1 H), 7.85 (s, 1 H), 7.82 (d, J = 8.0 Hz, 2 H), 7.70 (d, J = 8.0 Hz, 1 H), 7.49 (d, J = 8.0 Hz, 2 H), 6.98 (s, 1 H), 4.35 (s, 2 H), 3.27−3.20 (m, 2 H), 3.16−3.12 (m, 2 H), 2.64 (s, 3 H). ^{13}C NMR (126 MHz; DMSO-d_6): δ 154.6, 152.5, 143.7, 136.7, 133.0, 130.3, 126.8, 126.4, 121.7, 119.5, 119.3, 113.7, 110.2, 49.8, 47.4, 31.9, 19.5; one of the aminoquinoline carbons is not visible due to baseline broadening. ESIMS m/z (rel intensity) 317 (MH^+, 100). HRMS calcd for $C_{20}H_{21}N_4$, 317.1766; found, 317.1761.

*4-(2-(((2-Amino-4-methylquinolin-7-yl)methyl)amino)ethyl)-2-methylbenzonitrile Dihydrochloride (**25**).* Prepared from aldehyde **90** (0.072 g, 0.315 mmol) and phenethylamine **81** (0.065 g, 0.33 mmol), using general procedure 2, step 1. After concentration, reduction with $NaBH_4$ (0.017 g, 0.45 mmol), and workup, the secondary amine was protected with Boc_2O (0.072 g, 0.33 mmol), following general procedure 2, step 2. Workup and purification by flash column chromatography, eluting with a gradient of CH_2Cl_2 to 35% EtOAc in CH_2Cl_2, afforded the protected intermediate **92** (0.141 g, 95%). This was immediately deprotected with K_2CO_3 (0.082 g, 0.60 mmol) following general procedure 2, step 3. Following workup, the Boc group was removed using general procedure 2, step 4, to give the title compound as a white solid (0.096 g, 80%): mp 300−301 °C. ^{1}H NMR (500 MHz; DMSO-d_6): δ 14.15 (s, 1 H), 9.58 (s, 2 H), 9.02 (br s, 1 H), 8.20 (br s, 1 H), 8.05 (d, J = 7.5 Hz, 1 H), 7.82 (s, 1 H), 7.75 (d, J = 8.0 Hz, 1 H), 7.65 (br s, 1 H), 7.37 (s, 1 H), 7.29 (d, J = 8.0 Hz, 1 H), 6.95 (s, 1 H), 4.35 (s, 2 H), 3.26−3.15 (m, 2 H), 3.07 (t, J = 9.0 Hz, 2 H), 2.63 (s, 3 H), 2.47 (s, 3 H). ^{13}C NMR (126 MHz; DMSO-d_6): δ 143.4, 142.3, 133.3, 131.2, 127.5, 126.3, 121.9, 118.4, 113.7, 110.6, 49.9, 47.4, 31.8, 20.4, 19.4; four of the quinoline carbons and two of the aryl carbons are not visible due to baseline broadening. ESIMS m/z (rel intensity) 331 (MH^+, 100). HRMS calcd for $C_{21}H_{23}N_4$, 331.1922; found, 331.1924.

Purified NOS Enzyme Assays. Rat and human nNOS, murine macrophage iNOS, and human and bovine eNOS were recombinant enzymes (expressed in *Escherichia coli* and purified as reported previously).[44−46] The hemoglobin capture assay was used to measure nitric oxide production (to test for NOS inhibition). The assay was performed at 37 °C in HEPES buffer (100 mM with 10% glycerol, pH 7.4) in the presence of 10 μM L-arginine. NADPH (100 μM), $CaCl_2$ (0.83 mM), calmodulin (approximately 320 units/mL), H_4B (10 μM), and human oxyhemoglobin (3 μM) were also included in the assay mixture. For iNOS, the $CaCl_2$ and calmodulin were omitted and replaced with HEPES buffer (as neither are required for iNOS function). The assay was performed in 96-well plates using a Synergy 4 BioTek hybrid reader. Each well contained approximately 100 nM enzyme. The dispensing of NOS enzyme and hemoglobin were automated, and after 30 s (maximum delay), NO production was read by monitoring the absorbance at 401 nm (resulting from conversion of oxyhemoglobin to methemoglobin). Kinetic readouts were performed for 5 min. Each compound was assayed at least in duplicate, and seven to nine concentrations (500 μM to 50 nM or 100 μM to 10 nM for eNOS and iNOS; 50 μM to 5 nM for rat and human nNOS) were used to construct dose−response curves. IC_{50} values were calculated by nonlinear regression (variable slope, four parameters, bottom constraint set to 0 and top to 100) using GraphPad Prism software (reported standard error is reported for the $LogIC_{50}$), and K_i values were obtained from IC_{50} values, using the Cheng−Prusoff[47] equation [$K_i = IC_{50}/(1 + [S]/K_m)$] with the following K_m values: 1.3 μM (rat nNOS), 1.6 μM (human nNOS), 8.2 μM (murine macrophage iNOS), 1.7 μM (bovine eNOS), and 3.9 μM (human eNOS).[48]

Inhibitor Complex Crystal Preparation. The sitting drop vapor diffusion methods were used to grow crystals at 4 °C for the heme domains of rat nNOS (8 mg/mL containing 20 mM histidine), the human nNOS K301R/R354A/G357D mutant (10 mg/mL), and human eNOS (7 mg/mL). The crystal growth conditions are as described previously.[20] Fresh crystals were first passed stepwise through cryoprotectant solutions and then soaked with 5−10 mM inhibitor for 3−4 h at 4 °C before being flash cooled with liquid nitrogen and stored until data collection. The presence of an acetate ion near the heme active site in bovine eNOS had caused interference in the binding mode of some phenyl ether-linked aminoquinoline compounds.[15,20] The high concentration of magnesium acetate in the heNOS growth conditions may also introduce an acetate near the

DOI: 10.1021/acs.jmedchem.7b00835
J. Med. Chem. XXXX, XXX, XXX−XXX

active site that may influence the binding mode of inhibitors. To avoid having this acetate in the structure, the magnesium acetate in the cryoprotectant solution was replaced with $MgCl_2$.

X-ray Diffraction Data Collection, Data Processing, and Structural Refinement. The cryogenic (100 K) X-ray diffraction data were collected remotely at the Stanford Synchrotron Radiation Lightsource (SSRL) or Advanced Light Source (ALS) through the data collection control software Blu-Ice[49] and a crystal-mounting robot. When a Q315r CCD detector was used, 100−125° of data were typically collected with 0.5° per frame. If a Pilatus pixel array detector was used, 140−160° of fine-sliced data were collected with a 0.2° per frame. Raw CCD data frames were indexed, integrated, and scaled using iMOSFLM,[50] but the pixel array data were processed with XDS[51] and scaled with Aimless.[52] The binding of inhibitors was detected by initial difference Fourier maps calculated with REFMAC.[53] The inhibitor molecules were then modeled in Coot[54] and refined using REFMAC or PHENIX.[55] The crystal packing of the $MgCl_2$-soaked heNOS crystals was changed slightly, resulting in a symmetry change from the orthorhombic $P2_12_12_1$ reported previously[19] to monoclinic $P2_1$, with a β angle only 0.6−0.7° off compared to the original 90°. Therefore, a molecular replacement calculation with PHASER-MR[56] was needed to solve the structure. In the $P2_1$ space group, there are two heNOS dimers in the asymmetric unit. Disordering in portions of inhibitors bound in the NOS active sites was often observed, sometimes resulting in poor density quality. However, partial structural features were usually still visible if the contour level of the σA weighted $2m|F_o| - D|F_c|$ map was dropped to 0.5σ, which afforded the building of reasonable models into the disordered regions. Water molecules were added in PHENIX and checked by Coot. The TLS[57] protocol was implemented in the final stage of refinements with each subunit as one TLS group. The omit $F_o - F_c$ density maps were calculated by removing inhibitor coordinates from the input PDB file before running one more round of TLS refinement in PHENIX (simulated annealing protocol with a 2000 K initial temperature). The resulting map coefficients DELFWT and PHDELWT were used to generate maps. The refined structures were validated in Coot before deposition in the Protein Data Bank.

Caco-2 Permeability Assay. Caco-2 monolayer assays were performed by Cyprotex US, LLC (Watertown, MA), using standard procedures, as previously reported for aminoquinolines.[15]

■ ASSOCIATED CONTENT

Supporting Information

The Supporting Information is available free of charge on the ACS Publications website at DOI: 10.1021/acs.jmedchem.7b00835.

Crystallographic data collection and refinement statistics for rat and human nNOS and bovine eNOS-inhibitor crystal structures: rnNOS-**12** and hnNOS-**12**, rnNOS-**17** and hnNOS-**17**, rnNOS-**19** and hnNOS-**19**, rnNOS-**23** and beNOS-**23**, rnNOS-**25** and beNOS-**25**, rnNOS-**24**, beNOS-**24**, and heNOS-**24** crystal structures, and synthesis and analytical data for compounds **43**, **44**, **53**, **64**−**69** and **78**−**82** (PDF)

Molecular formula strings (CSV)

Accession Codes

X-ray crystal structures described in this study have been deposited in the Protein Data Bank. We will release the atomic coordinates and experimental data upon article publication under the following accession codes: rnNOS-**8**, 5VUI; rnNOS-**12**, 5VUJ; rnNOS-**13**, 5VUK; rnNOS-**15**, 5VUL; rnNOS-**16**, 5VUM; rnNOS-**17**, 5VUN; rnNOS-**18**, 5VUO; rnNOS-**19**, 5VUP; rnNOS-**21**, 5VUQ; rnNOS-**22**, 5VUR; rnNOS-**23**, 5VUS; rnNOS-**24**, 5VUT; rnNOS-**25**, 5VUU; hnNOS-**8**, 5VUV; hnNOS-**12**, 5VUW; hnNOS-**13**, 5VUX; hnNOS-**15**, 5VUY; hnNOS-**16**, 5VUZ; hnNOS-**17**, 5VV0; hnNOS-**18**, 5VV1; hnNOS-**19**, 5VV2; hnNOS-**21**, 5VV3; hnNOS-**22**, 5VV4; hnNOS-**25**, 5VV5; beNOS-**15**, 5VV6; beNOS-**16**, 5VV7; beNOS-**21**, 5VVN; beNOS-**22**, 5VV8; beNOS-**24**, 5VV9; beNOS-**23**, 5VVG; beNOS-**25**, 5VVA; heNOS-**22**, 5VVB; heNOS-**24**, 5VVD; heNOS-**25**, 5VVC.

■ AUTHOR INFORMATION

Corresponding Authors

*For R.B.S.: phone, +1 847 491 5653; fax, +1 847 491 7713; E-mail, Agman@chem.northwestern.edu.

*For T.L.P.: phone, +1 949 824 7020; E-mail, poulos@uci.edu.

ORCID

Thomas L. Poulos: 0000-0002-5648-3510

Richard B. Silverman: 0000-0001-9034-1084

Author Contributions

⊥A.V.P. and M.A.C. contributed equally to this work.

Notes

The authors declare no competing financial interest.

■ ACKNOWLEDGMENTS

We thank the National Institutes of Health (R01GM049725, to R.B.S., GM057353 to T.L.P., and F32GM109667 to M.A.C.) for generous support of this work. A.P. was supported by a Lambert Fellowship (Chemistry of Life Processes Institute, Northwestern University) and by the Katherine L. Kreighbaum Scholarship (Northwestern University). L.J.R. is currently supported on NIH GM081568 and NSF grant 13-573. P.M. is supported by grants UNCE 204011 and PRVOUK P24/LF1/3 from Charles University, Prague, Czech Republic. A.P. and M.A.C. thank Saman Shafaie and Dr. S. Habibi Goudarzi for assistance with HRMS experiments, and Drs. Arsen Gaisin and Neha Malik of the Center for Molecular Innovation and Drug Discovery (Northwestern University) for valuable assistance with preparative HPLC. This work made use of IMSERC at Northwestern University, which has received support from the Soft and Hybrid Nanotechnology Experimental (SHyNE) Resource (NSF NNCI-1542205), the State of Illinois, and the International Institute for Nanotechnology (IIN). H.L. thanks Carla Plaza for her assistance in NOS protein expression and purification; the purified samples were used in both crystallography and enzyme assays. We also thank the SSRL and ALS beamline staff for their support during remote X-ray diffraction data collection. Off-target K_i determinations (CNS counterscreening) were generously provided by the National Institute of Mental Health's Psychoactive Drug Screening Program, (contract no. HHSN-271-2013-00017-C, NIMH PDSP), directed by Dr. Bryan L. Roth (University of North Carolina at Chapel Hill) and project officer Jamie Driscoll (NIH).

■ ABBREVIATIONS USED

NO, nitric oxide; nNOS, neuronal nitric oxide synthase; eNOS, endothelial nitric oxide synthase; iNOS, inducible nitric oxide synthase; rnNOS, rat nNOS; hnNOS, human nNOS; beNOS, bovine eNOS; heNOS, human eNOS; miNOS, murine macrophage iNOS; P_{app}, apparent permeability; HEPES, 4-(2-hydroxyethyl)-1-piperazineethanesulfonic acid; PDSP, psychoactive drug screening program; FMN, flavin mononucleotide; H_4B, (6*R*)-5,6,7,8-tetrahydrobiopterin; PSA, polar surface area

DOI: 10.1021/acs.jmedchem.7b00835
J. Med. Chem. XXXX, XXX, XXX−XXX

REFERENCES

(1) Hebert, L. E.; Scherr, P. A.; Bienias, J. L.; Bennett, D. A.; Evans, D. A. Alzheimer disease in the US population: prevalence estimates using the 2000 census. *Arch. Neurol.* **2003**, *60*, 1119−1122.

(2) Torreilles, F.; Salman-Tabcheh, S.; Guerin, M.; Torreilles, J. Neurodegenerative disorders: the role of peroxynitrite. *Brain Res. Rev.* **1999**, *30*, 153−163.

(3) Zhang, L.; Dawson, V. L.; Dawson, T. M. Role of nitric oxide in Parkinson's disease. *Pharmacol. Ther.* **2006**, *109*, 33−41.

(4) Huang, Z.; Huang, P. L.; Panahian, N.; Dalkara, T.; Fishman, M. C.; Moskowitz, M. A. Effects of cerebral ischemia in mice deficient in neuronal nitric oxide synthase. *Science* **1994**, *265*, 1883−1885.

(5) Dorheim, M.-A.; Tracey, W. R.; Pollock, J. S.; Grammas, P. Nitric oxide synthase activity is elevated in brain microvessels in Alzheimer's disease. *Biochem. Biophys. Res. Commun.* **1994**, *205*, 659−665.

(6) Kim, K. H.; Kim, J. I.; Han, J. A.; Choe, M. A.; Ahn, J. H. Upregulation of neuronal nitric oxide synthase in the periphery promotes pain hypersensitivity after peripheral nerve injury. *Neuroscience* **2011**, *190*, 367−378.

(7) Maccallini, C.; Amoroso, R. Targeting neuronal nitric oxide synthase as a valuable strategy for the therapy of neurological disorders. *Neural Regener. Res.* **2016**, *11*, 1731−1734.

(8) Mukherjee, P.; Cinelli, M. A.; Kang, S.; Silverman, R. B. Development of nitric oxide synthase (NOS) inhibitors for neurodegenerative diseases and neuropathic pain. *Chem. Soc. Rev.* **2014**, *43*, 6814−6838.

(9) Siddhanta, U.; Presta, A.; Fan, B.; Wolan, D.; Rousseau, D. L.; Stuehr, D. J. Domain swapping in inducible NO synthase: electron transfer occurs between flavin and heme groups located on adjacent subunits in the dimer. *J. Biol. Chem.* **1998**, *273*, 18950−18958.

(10) Rosen, G. M.; Tsai, P.; Pou, S. Mechanism of free-radical generation by nitric oxide synthase. *Chem. Rev.* **2002**, *102*, 1191−1199.

(11) Delker, S. L.; Ji, H.; Li, H.; Jamal, J.; Fang, J.; Xue, F.; Silverman, R. B.; Poulos, T. L. Unexpected binding modes of nitric oxide synthase inhibitors effective in the prevention of cerebral palsy. *J. Am. Chem. Soc.* **2010**, *132*, 5437−5442.

(12) Wang, H.-Y.; Qin, Y.; Li, H.; Roman, L. J.; Martásek, P.; Poulos, T. L.; Silverman, R. B. Potent and selective human neuronal nitric oxide synthase inhibition by optimization of the 2-aminopyridine-based scaffold with a pyridine linker. *J. Med. Chem.* **2016**, *59*, 4913−4925.

(13) Mukherjee, P.; Li, H.; Sevrioukova, I.; Chreifi, G.; Martásek, P.; Roman, L. J.; Poulos, T. L.; Silverman, R. B. Novel 2,4-disubstituted pyrimidines as potent, selective, and cell-permeable inhibitors of neuronal nitric oxide synthase. *J. Med. Chem.* **2015**, *58*, 1067−1088.

(14) Cinelli, M. A.; Li, H.; Chreifi, G.; Martásek, P.; Roman, L. J.; Poulos, T. L.; Silverman, R. B. Simplified 2-aminoquinoline-based scaffold for potent and selective neuronal nitric oxide synthase inhibition. *J. Med. Chem.* **2014**, *57*, 1513−1530.

(15) Cinelli, M. A.; Li, H.; Pensa, A. V.; Kang, S.; Martásek, P.; Roman, L. J.; Poulos, T. L.; Silverman, R. B. Phenyl ether- and aniline-containing 2-aminoquinolines as potent and selective inhibitors of neuronal nitric oxide synthase. *J. Med. Chem.* **2015**, *58*, 8694−8712.

(16) Kobayashi, Y.; Ikeda, K.; Shinozuka, K.; Nara, Y.; Yamori, Y.; Hattori, K. L-nitroarginine increases blood pressure in the rat. *Clin. Exp. Pharmacol. Physiol.* **1991**, *18*, 397−399.

(17) Wilcock, D. M.; Lewis, M. R.; Van Nostrand, W. E.; Davis, J.; Previti, M. L.; Gharkholonarehe, N.; Vitek, M. P.; Colton, C. A. Progression of amyloid pathology to Alzhemer's disease pathology in an amyloid precursor protein transgenic mouse model by removal of nitric oxide synthase 2. *J. Neurosci.* **2008**, *28*, 1537−1545.

(18) Li, M.; Dai, F.; Du, X.; Yang, Q.; Chen, Y. Neuroprotection by silencing iNOS expression in a 6-OHDA model of Parkinson's disease. *J. Mol. Neurosci.* **2012**, *48*, 225−233.

(19) Besnard, J.; Ruda, G. F.; Setola, V.; Abecassis, K.; Rodriguiz, R. M.; Huang, X. P.; Norval, S.; Sassano, M. F.; Shin, A. I.; Webster, L. A.; Simeons, F. R.; Stojanovski, L.; Prat, A.; Seidah, N. G.; Constam, D. B.; Bickerton, G. R.; Read, K. D.; Wetsel, W. C.; Gilbert, I. H.; Roth, B. L.; Hopkins, A. L. Automated design of ligands to polypharmacological profiles. *Nature* **2012**, *492*, 215−220.

(20) Cinelli, M. A.; Li, H.; Chreifi, G.; Poulos, T. L.; Silverman, R. B. Nitrile in the hole: discovery of a small auxiliary pocket in neuronal nitric oxide synthase leading to the development of potent and selective 2-aminoquinoline inhibitors. *J. Med. Chem.* **2017**, *60*, 3958−3978.

(21) Li, H.; Jamal, J.; Plaza, C.; Pineda, S. H.; Chreifi, G.; Jing, Q.; Cinelli, M. A.; Silverman, R. B.; Poulos, T. L. Crystal structures of human constitutive nitric oxide synthases. *Acta Crystallogr., Sect. D: Biol. Crystallogr.* **2014**, *70*, 2667−2674.

(22) Xue, F.; Li, H.; Fang, J.; Roman, L. J.; Martásek, P.; Poulos, T. L.; Silverman, R. B. Peripheral but crucial: A hydrophobic pocket (Tyr706, Leu337, and Met336) for potent and selective inhibition of neuronal nitric oxide synthase. *Bioorg. Med. Chem. Lett.* **2010**, *20*, 6258−6261.

(23) Kang, S.; Li, H.; Tang, W.; Martásek, P.; Roman, L. J.; Poulos, T. L.; Silverman, R. B. 2-Aminopyridines with a truncated side chain to improve human neuronal nitric oxide synthase inhibitory potency and selectivity. *J. Med. Chem.* **2015**, *58*, 5548−5560.

(24) Ji, H.; Li, H.; Martásek, P.; Roman, L. J.; Poulos, T. L.; Silverman, R. B. Discovery of highly potent and selective inhibitors of neuronal nitric oxide synthase by fragment hopping. *J. Med. Chem.* **2009**, *52*, 779−797.

(25) Jones, L. H.; Summerhill, N. W.; Swain, N. A.; Mills, J. E. Aromatic chloride to nitrile transformation: medicinal and synthetic chemistry. *MedChemComm* **2010**, *1*, 309−318.

(26) Romera, J. L.; Cid, J. M.; Trabanco, A. A. Potassium iodide catalysed monoalkylation of anilines under microwave irradiation. *Tetrahedron Lett.* **2004**, *45*, 8797−8800.

(27) Inglis, S.; Jones, R.; Fritz, D.; Stojkoski, C.; Booker, G.; Pyke, S. Synthesis of 5-, 6- and 7-subsituted -2-aminoquinolines as SH3 domain ligands. *Org. Biomol. Chem.* **2005**, *3*, 2543−2557.

(28) Salvatore, R. N.; Nagle, A. S.; Jung, K. W. Cesium Effect: High chemoselectivity in direct *N*-alkylation of amines. *J. Org. Chem.* **2002**, *67*, 674−683.

(29) Ahmed, G.; Bohnstedt, A.; Breslin, H. J.; Burke, J.; Curry, M. A.; Diebold, J. L.; Dorsey, B.; Dugan, B. J.; Feng, D.; Gingrich, D. E.; Guo, T.; Ho, K.-K.; Learn, K. S.; Lisko, J. G.; Liu, R.-Q.; Mesaros, E. F.; Milkiewicz, K.; Ott, G. R.; Parrish, J.; Theroff, J. P.; Thieu, T. V.; Tripathy, R.; Underiner, T. L.; Wagner, J. C.; Weinberg, L.; Wells, G. J.; You, M.; Zificsak, C. A. Fused Bicyclic Derivatives of 2,4-Diaminopyrimidine as ALK and c-Met Kinase Inhibitors. WO2008/051547, May 2, 2008.

(30) Lopchuk, J. M.; Hughes, P.; Gribble, G. W. What controls regiochemistry in 1,3-dipolar cycloadditions of munchnones with nitrostyrenes? *Org. Lett.* **2013**, *15*, 5218−5221.

(31) Guedat, P.; Berecibar, A.; Ciapetti, P.; Vekata Pithani, S.; Trouche, N.; Vivalis, F. Hydantoin and Thiohydantoin Derivatives as Antiviral Drugs. EP2664616, November 20, 2013.

(32) Senecal, T. D.; Shu, W.; Buchwald, S. L. A general, practical palladium-catalyzed cyanation of (hetero)aryl chlorides and bromides. *Angew. Chem., Int. Ed.* **2013**, *52*, 10035−10039.

(33) Charrier, J.-D.; Binch, H. M., Hurley, D. J.; Cleveland, T.; Joshi, P.; Fanning, L. T. D.; Pinder, J.; O'Donnell, M.; Virani, A. N.; Knegtel, R. M. A.; Durrant, S. J.; Young, S. C.; Storck, P.-H.; Kay, D.; Reaper, P. M. Compounds Useful as Inhibitors of ATR Kinase. WO2011/143426, November 17, 2011.

(34) Adams, N. D.; Chuadhari, A. M.; Kiesow, T. J.; McSherry, A. K.; Moore, M. L.; Parrish, C. A.; Reif, A. J.; Ridgers, L. H. Spirocyclic Piperidine Derivatives for Use as Fatty Acid Synthase Inhibitors. WO2014/008223, January 9, 2014.

(35) Brown, W.; Johnstone, S.; Larecque, D. Benzimidiazole Derivatives as Vanilloid Receptor Antagonists, Their Preparation, Pharmaceutical Compositions, and Use in Therapy. WO2008/018827, February 14, 2008.

(36) Runyon, S. P.; Mosier, P. D.; Roth, B. L.; Glennon, R. A.; Westkaemper, R. B. Potential modes of interaction of 9-aminomethyl-9,10-dihydroanthracene (AMDA) derivatives with the 5-HT2A

DOI: 10.1021/acs.jmedchem.7b00835
J. Med. Chem. XXXX, XXX, XXX−XXX

receptor: ligand structure-affinity relationship, receptor mutagenesis and receptor modeling investigation. *J. Med. Chem.* **2008**, *51*, 6808−6828.
(37) Silverman, R. B.; Cinelli, M. A.; Pensa, A. V. 2-Aminoquinoline Compounds for Potent and Selective Neuronal Nitric Oxide Synthase Inhibition. US Patent 9,663,468, May 30, 2017.
(38) Yin, J.; Xiang, B.; Huffman, M. A.; Raab, C. E.; Davies, I. W. A general and efficient 2-amination of pyridines and quinolines. *J. Org. Chem.* **2007**, *72*, 4554−4557.
(39) Ueda, T.; Konishi, H.; Manabe, K. Palladium-catalyzed reductive carbonylation of aryl halides with *N*-formylsaccharin as a CO source. *Angew. Chem., Int. Ed.* **2013**, *52*, 8611−8615.
(40) Fedorov, R.; Vasan, R.; Ghosh, D.; Schlichting, I. Structures of nitric oxide synthase isoforms complexed with the inhibitor AR-R17477 suggest a rational basis for specificity and inhibitor design. *Proc. Natl. Acad. Sci. U. S. A.* **2004**, *101*, 5892−5897.
(41) Smith, G. F. Designing drugs to avoid toxicity. *Prog. Med. Chem.* **2011**, *50*, 1−47.
(42) Fleming, F. F.; Yao, L.; Ravikumar, P. C.; Funk, L.; Shook, B. C. Nitrile-containing pharmaceuticals: efficacious roles of the nitrile pharmacophore. *J. Med. Chem.* **2010**, *53*, 7902−7917.
(43) Lundquist, S.; Renftel, M.; Brillault, J.; Fenart, L.; Cecchelli, R.; Dehouck, M. P. Prediction of drug transport through the blood-brain barrier in vivo: a comparison between two in vitro cell models. *Pharm. Res.* **2002**, *19*, 976−981.
(44) Roman, L. J.; Sheta, E. A.; Martásek, P.; Gross, S. S.; Liu, Q.; Masters, B. S. S. High-level expression of functional rat neuronal nitric oxide synthase in *Escherichia coli*. *Proc. Natl. Acad. Sci. U. S. A.* **1995**, *92*, 8428−8432.
(45) Hevel, J. M.; White, K. A.; Marletta, M. A. Purification of the inducible murine macrophage nitric oxide synthase: identification as a flavoprotein. *J. Biol. Chem.* **1991**, *266*, 22789−22791.
(46) Gerber, N. C.; Ortiz de Montellano, P. R. Neuronal nitric oxide synthase: expression in *Escherichia coli*, irreversible inhibition by phenyldiazene, and active site topology. *J. Biol. Chem.* **1995**, *270*, 17791−17796.
(47) Cheng, Y.-C.; Prusoff, W. H. Relationship between the inhibition constant (K_i) and the concentration of the inhibitor which causes 50% inhibition (IC50) of an enzymatic reaction. *Biochem. Pharmacol.* **1973**, *22*, 3099−3108.
(48) Leber, A.; Hemmens, B.; Klosch, B.; Goessler, W.; Raber, G.; Mayer, B.; Schmidt, K. Characterization of recombinant human endothelial nitric-oxide synthase purified from the yeast *Pichia pastoris*. *J. Biol. Chem.* **1999**, *274*, 37658−37665.
(49) McPhillips, T. M.; McPhillips, S. E.; Chiu, H. J.; Cohen, A. E.; Deacon, A. M.; Ellis, P. J.; Garman, E.; Gonzalez, A.; Sauter, N. K.; Phizackerley, R. P.; Soltis, S. M.; Kuhn, P. Blu-Ice and the Distributed Control System: software for data acquisition and instrument control at macromolecular crystallography beamlines. *J. Synchrotron Radiat.* **2002**, *9*, 401−406.
(50) Battye, T. G. G.; Kontogiannis, L.; Johnson, O.; Powell, H. R.; Leslie, A. G. W. iMOSFLM: a new graphical interface for diffraction-image processing with MOSFLM. *Acta Crystallogr., Sect. D: Biol. Crystallogr.* **2011**, *67*, 271−281.
(51) Kabsch, W. XDS. *Acta Crystallogr., Sect. D: Biol. Crystallogr.* **2010**, *66*, 125−132.
(52) Evans, P. R. Scaling and assessment of data quality. *Acta Crystallogr., Sect. D: Biol. Crystallogr.* **2006**, *62*, 72−82.
(53) Murshudov, G. N.; Vagin, A. A.; Dodson, E. J. Refinement of macromolecular structures by the maximum-likelihood method. *Acta Crystallogr., Sect. D: Biol. Crystallogr.* **1997**, *53*, 240−255.
(54) Emsley, P.; Cowtan, K. Coot: model-building tools for molecular graphics. *Acta Crystallogr., Sect. D: Biol. Crystallogr.* **2004**, *60*, 2126−2132.
(55) Adams, P. D.; Afonine, P. V.; Bunkoćzi, G.; Chen, V. B.; Davis, I. W.; Echols, N.; Headd, J. J.; Hung, L.-W.; Kapral, G. J.; Grosse-Kunstleve, R. W.; McCoy, A. J.; Moriarty, N. W.; Oeffner, R.; Read, R. J.; Richardson, D. C.; Richardson, J. S.; Terwilliger, T. C.; Zwart, P. H. PHENIX: a comprehensive Python-based system for macromolecular structure solution. *Acta Crystallogr., Sect. D: Biol. Crystallogr.* **2010**, *66*, 213−221.
(56) McCoy, A. J.; Grosse-Kunstleve, R. W.; Adams, P. D.; Winn, M. D.; Storoni, L. C.; Read, R. J. Phaser crystallographic software. *J. Appl. Crystallogr.* **2007**, *40*, 658−674.
(57) Winn, M. D.; Isupov, M. N.; Murshudov, G. N. Use of TLS parameters to model anisotropic displacements in macromolecular refinement. *Acta Crystallogr., Sect. D: Biol. Crystallogr.* **2001**, *57*, 122−133.

DOI: 10.1021/acs.jmedchem.7b00835
J. Med. Chem. XXXX, XXX, XXX−XXX